

1 **Exploring the sources of light-absorbing carbonaceous aerosols by integrating observational**  
2 **and modeling results: insights from Northeast China**

3 Yuan Cheng<sup>1</sup>, Xu-bing Cao<sup>1</sup>, Sheng-qiang Zhu<sup>2</sup>, Zhi-qing Zhang<sup>1</sup>, Jiu-meng Liu<sup>1,\*</sup>, Hong-liang  
4 Zhang<sup>2</sup>, Qiang Zhang<sup>3</sup> and Ke-bin He<sup>4</sup>

5 <sup>1</sup> State Key Laboratory of Urban Water Resource and Environment, School of Environment, Harbin  
6 Institute of Technology, Harbin, 150090, China

7 <sup>2</sup> Department of Environmental Science and Engineering, Fudan University, Shanghai 200438,  
8 China

9 <sup>3</sup> Ministry of Education Key Laboratory for Earth System Modeling, Department of Earth System  
10 Science, Tsinghua University, Beijing, 100084, China

11 <sup>4</sup> State Key Joint Laboratory of Environment Simulation and Pollution Control, School of  
12 Environment, Tsinghua University, Beijing, 100084, China

13 \* Corresponding author. Jiu-meng Liu (jiumengliu@hit.edu.cn).

14 **Abstract**

15 Light-absorbing carbonaceous aerosols are important contributors to both air pollution and radiative  
16 forcing. However, their abundances and sources remain poorly constrained, as can be seen from  
17 the frequently-identified discrepancies between the observed and modeled results. In this study, we  
18 focused on elemental carbon (EC, as a measure of black carbon) and light-absorbing organic carbon  
19 (i.e., BrC) in Northeast China, a new targeted region of the latest clean air actions in China. Three  
20 campaigns were conducted during 2018–2021 in Harbin, covering distinct meteorological  
21 conditions and emission features. Various analytical methods were first evaluated, and the mass  
22 concentrations of both BrC and EC were validated. The validated BrC and EC measurement results  
23 were then used for source apportionment, together with other species including tracers (e.g.,  
24 levoglucosan). The observation-based results suggested that despite the frigid winter in Harbin, the  
25 formation of secondary organic carbon (SOC) was enhanced at high levels of relative humidity (RH).  
26 This enhancement could also be captured by an air quality model incorporating heterogeneous

27 chemistry. However, the model failed to reproduce the observed abundances of SOC, with  
28 significant underestimations regardless of RH levels. In addition, agricultural fires effectively  
29 increased the observation-based primary organic carbon (POC) concentrations and POC to EC ratios.  
30 Such roles of agricultural fires were not captured by the model, pointing to substantial  
31 underestimation of open burning emissions by the inventory. This problem merits particular  
32 attention for Northeast China, given its massive agricultural sector.

## 33 **1. Introduction**

34 Black carbon (BC) and light-absorbing organic carbon, i.e., brown carbon (BrC), are important  
35 contributors to not only haze pollution but also positive radiative forcing (Bond et al., 2013; Laskin  
36 et al., 2015). While their environmental effects are usually predicted by chemical transport and  
37 radiative transfer models, field observational results are necessary to constrain their simulated  
38 spatial distributions and temporal variations (Koch et al., 2009; Samset et al., 2014; Stohl et al.,  
39 2015; Wang et al., 2018; Gao et al., 2022). For example, several studies suggested that to improve  
40 the agreement between simulated and observed BC concentrations, the BC lifetime should be on  
41 the lower end of those assumed in current models (e.g., Samset et al., 2014). However, the  
42 observational data on both BC and BrC are still subject to considerable uncertainties, largely due to  
43 the lack of reference material and method for both species (Baumgardner, et al., 2012; Petzold et al.,  
44 2013; Lack et al., 2014).

45 The measurement techniques for BC mass typically fall into four categories, i.e., thermal-  
46 optical (Chow et al., 2007; Cavalli et al., 2010), light absorption (Petzold et al., 2005), laser-induced  
47 incandescence (LII; Schwartz et al., 2006) and aerosol mass spectrometric methods (Onasch et al.,  
48 2012). These approaches are based on different measurement principles, depending on the targeted  
49 properties of BC (Petzold et al., 2013). For example, in the thermal-optical method, a particle-laden  
50 filter is heated in an inert (i.e., He) and oxidizing (i.e., He/O<sub>2</sub>) atmosphere sequentially to volatilize  
51 and combust the deposited carbonaceous components. BC typically evolves after organic matters  
52 due to its higher thermal stability. In addition, BC is strongly light-absorbing and thus its evolution  
53 could lead to a rapid increase of the filter transmittance signal, which is typically monitored in the  
54 spectral range of red light. Then based on the evolution patterns of the carbon and transmittance

55 signals, BC mass could be determined as the amount of carbon evolving during a specific segment  
56 of thermal-optical analysis (Cavalli et al., 2010). In addition to the thermal-optical method, BC mass  
57 could also be determined based on the aerosol light absorption coefficient (in  $Mm^{-1}$ ; Moosmüller et  
58 al., 2009), carbon ion signals in a mass spectrum measured by a Soot Particle Aerosol Mass  
59 Spectrometer (SP-AMS; Onasch et al., 2012), or the incandescent radiation emitted during fast  
60 heating, boiling and evaporation of BC in a LII instrument (Moteki and Kondo, 2010). The  
61 multitude of measurement principles result in considerable discrepancies in BC results among  
62 different methods, and interestingly, the discrepancies were usually not constant even for the same  
63 study (Buffaloe et al., 2014; Sharma et al., 2017; Corbin et al., 2019; Li et al., 2019; Pileci et al.,  
64 2021; Tinorua et al., 2024). For example, results from the LII and thermal-optical methods were  
65 found to show BC ratios varying between 0.5 and 1.2 for several background sites in Europe, with  
66 unclear reasons for the variability in discrepancies (Pileci et al., 2021).

67         Similar to BC, different methods co-exist for the measurement of BrC. For example, BrC's  
68 light absorption coefficient is usually determined based on extract of filter sample (Hecobian et al.,  
69 2010) or total aerosol absorption (Yang et al., 2009). Different relationships have been identified  
70 between the results from these two approaches, e.g., strong correlation and close agreement (Zeng  
71 et al., 2022), moderate to strong correlations with considerable differences in the absolute values  
72 (Kumar et al., 2018; Cheng et al., 2021b), and little correlation (Chen et al., 2022). However, factors  
73 responsible for the inconsistent relationships remain poorly understood. In addition, the  
74 measurement of BrC mass is also challenging. This is particularly the case for studies using organic  
75 solvents (e.g., methanol) to extract or isolate BrC. A major difficulty is that the amount of BrC  
76 dissolved in organic solvents could not be directly measured, whereas the indirect approaches are

77 still under debate regarding the possible artifacts (Yan et al., 2020). For example, when determining  
78 BrC mass as the difference in total carbon concentration between untreated and extracted filters, the  
79 result could be biased high due to the loss of insoluble BC during extraction.

80         Nonetheless, the measurement methods of BC and BrC require further refinements to provide  
81 more robust constraints on the modelling results. Such efforts are especially necessary for China,  
82 given its more complex emission sources compared to North America and Europe. Here we focus  
83 on Harbin, a representative megacity in Northeast China. With the improvement of air quality in  
84 other regions such as the North China Plain (Xiao et al., 2021; Wang et al., 2023b), Northeast China  
85 was targeted by the national-level clean air policy for the first time in 2021 (State Council, 2021).  
86 This policy, i.e., the *Circular on Further Promoting the Pollution Prevention and Control Battle*,  
87 proposed an ambitious goal of eliminating heavy or severe air pollution events in Northeast China  
88 and other key regions. In addition, Harbin will be hosting the 9<sup>th</sup> Asia Winter Games in February of  
89 2025, which posed another motivation for cleaning the air in Northeast China. However, the  
90 roadmap for air quality improvement was to some extent masked for Harbin as well as other cities  
91 in Northeast China, given that the sources and formation mechanisms of haze pollution were far  
92 from being well understood with limited studies (e.g., Zhang et al., 2020; Wu et al., 2020; Ning et  
93 al., 2022).

94         This study aimed at understanding the sources of light-absorbing carbon in Harbin, based on a  
95 synthesis of field observation and air quality modeling. We started with the coordinated  
96 determination of BrC and BC masses in filter samples, followed by source apportionment using the  
97 validated observational results. Then we used the observation-based BrC and BC source attributions  
98 to constrain the predictions by an air quality model, with focuses on the model vs. observation

99 discrepancies and the drivers at play. This study provided implications for further efforts to  
100 understand the haze pollution in Northeast China, with respect to both the measurement and  
101 simulation of carbonaceous aerosols.

## 102 **2. Methods**

### 103 **2.1 Field observation**

104 A total of 486 fine particulate matter (PM<sub>2.5</sub>) samples were collected on a daily basis at an  
105 urban site in Harbin during three recent campaigns (Table 1). The sampling was performed on the  
106 campus of Harbin Institute of Technology, using a portable sampler (MiniVol; Airmetrics, OR, USA)  
107 operated at a flow rate of 5 L/min with quartz-fiber filters (Pall Corporation, NY, USA). For each  
108 sample, a half of the filter was measured for water-soluble inorganic ions and levoglucosan, using  
109 a Dionex ion chromatography system (ICS-5000<sup>+</sup>; Thermo Fisher Scientific Inc., MA, USA). The  
110 other half was cut into two punches for the determination of organic carbon (OC) and elemental  
111 carbon (EC, as a measure of BC mass), using a thermal/optical carbon analyzer (DRI-2001;  
112 Atmoslytic Inc., CA, USA). The first punch was measured directly, while the second punch was  
113 immersed in methanol (Fisher Scientific Company L.L.C., NJ, USA) for an hour without stirring or  
114 sonication, dried in air for another hour, and then analyzed. All the pairs of untreated and extracted  
115 punches were measured deploying the IMRPOVE-A temperature protocol, with selected pairs also  
116 analyzed using NIOSH (Table 1). In addition, wavelength-resolved light absorption coefficients  
117 ( $b_{\text{abs}}$ ) of the methanol extracts were quantified using a spectrophotometer (Ocean Optics Inc., FL,  
118 USA) coupled with a 2.5m long liquid waveguide capillary cell (LWCC; World Precision Instrument,  
119 FL, USA). Samples strongly impacted by firework emissions ( $N = 2, 3$  and  $6$  for the three campaigns,  
120 respectively) during the Chinese New Year periods were not further investigated in this study. More

121 details of the field observations were presented in Cheng et al. (2021a and 2022).

122 **Table 1.** Summary of PM<sub>2.5</sub> samples involved in this study. *N* indicates the number of samples from  
123 each campaign. For each sample, both the untreated and extracted punches were used for thermal-  
124 optical analysis. *NP*<sub>IMPROVE-A</sub> indicates the number of punch pairs analyzed by the IMPROVE-A  
125 temperature protocol. *NP*<sub>NIOSH</sub> was defined similarly. The split of OC and EC was based on the  
126 transmittance charring correction for both protocols.

Measurement period	Main features <sup>a</sup>	<i>N</i>	<i>NP</i> <sub>IMPROVE-A</sub>	<i>NP</i> <sub>NIOSH</sub> <sup>b</sup>
October 16, 2018–April 14, 2019	Fires in late winter	180	180	180
October 16, 2019–February 4, 2020 <sup>c</sup>	Humid winter	112	112	73
October 17, 2020–April 30, 2021	Fires in April	194	194	86

127 <sup>a</sup> Main features of the campaigns were presented briefly in Figure S1, and described in detail in  
128 Cheng et al. (2021a and 2022).

129 <sup>b</sup> The selection of samples analyzed by both protocols will be explained in detail in Section 3.2.

130 <sup>c</sup> The 2019–2010 campaign covered a relatively short period due to the lockdown policy associated  
131 with the outbreak of COVID-19.

## 132 2.2 Air quality modeling

133 A revised Community Multi-scale Air Quality (CMAQ) model was used to simulate OC and  
134 EC in Harbin. Compared to the original version (5.0.1), a major update of the revised model was  
135 the addition of new pathways for secondary organic aerosol (SOA) production, i.e., photochemical  
136 and heterogeneous oxidation of isoprene epoxydiols, methacrylic acid epoxide, glyoxal and  
137 methylglyoxal (Ying et al., 2015). Previous studies suggested that the revised CMAQ could  
138 generally reproduce the observed meteorological conditions and PM<sub>2.5</sub> concentrations on a national  
139 scale in China (Hu et al., 2016a; Wang et al., 2020). However, the model performance remained  
140 inconclusive for PM<sub>2.5</sub> compositions in specific regions. In this study, the modeling was performed  
141 over East China with a horizontal resolution of 36 × 36 km for the 2020–2021 measurement period.  
142 The simulation results were extracted for the grid cell where the sampling site is located at, and then  
143 compared with the observational results.

## 144 3. Results and discussion

### 145 3.1 Validation of BrC measurement results

146 Extracting filter samples by methanol was a common approach to measure brown carbon.  
147 While the light absorption by BrC could be readily determined using the methanol extracts, it  
148 remains challenging to quantify the mass concentration of BrC, i.e., methanol-soluble OC (MSOC).  
149 Unlike water-soluble OC (WSOC), the measurement of MSOC could not be directly done using a  
150 Total Organic Carbon analyzer and instead required indirect methods. For example, a four-step  
151 procedure was developed by Chen et al. (2017), including drying the methanol extract in a nitrogen  
152 flow, re-dissolving the residues in a small amount of methanol (100  $\mu$ L), spiking a pre-baked filter  
153 punch (prepared for thermal-optical carbon analyzer) with a known volume of the new extract (20  
154  $\mu$ L), and measuring the total carbon (TC) in the spiked filter after drying as MSOC. A simpler  
155 approach was to determine MSOC as the difference in TC (or OC) concentrations between the  
156 untreated and extracted filter punches. This method was initially developed by Chen and Bond  
157 (2010), with a substantial concern being the loss of insoluble carbon (e.g., EC) during extraction.  
158 However, this artifact was difficult to evaluate, largely due to the lack of reference method for the  
159 measurement of EC mass (Petzold et al., 2013).

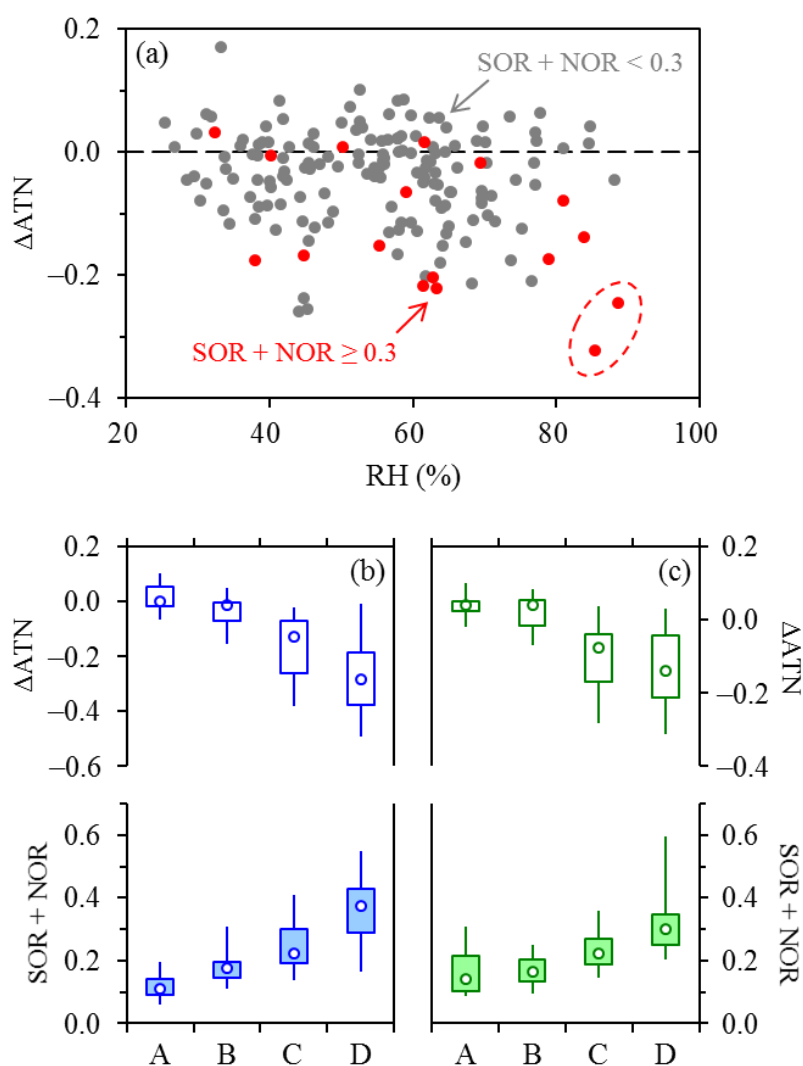
160 In addition to EC mass, optical attenuation (ATN) retrieved from the carbon analyzer could be  
161 an alternative criterion for estimating the extraction-induced loss of insoluble carbon. ATN was  
162 calculated as  $\ln(I_{\text{final}}/I_{\text{initial}})$ , where  $I_{\text{initial}}$  and  $I_{\text{final}}$  indicates the filter transmittance signals ( $I$ )  
163 measured at the beginning and end of thermal-optical analysis, respectively.  $I_{\text{initial}}$  was lower than  
164  $I_{\text{final}}$  mainly due to the absorption by light-absorbing aerosols (e.g., EC and BrC) and scattering or  
165 more specifically backward scattering (Petzold et al., 2005) by the deposited particles (e.g.,  
166 inorganic ions and non-absorbing OC). Given that  $I$  was monitored at a wavelength of 632 nm, only



167 strongly-absorbing BrC could influence  $I_{\text{initial}}$  and thus ATN through absorption, while SOA could  
168 be considered almost non-absorbing (Lambe et al., 2013; Liu et al., 2015, 2016a). Thus we suggest  
169 that (i) decrease of ATN after extraction, if occurred, could be mainly attributed to three possible  
170 factors, including loss of EC, removal of strongly-absorbing BrC and removal of scattering  
171 compounds such as SOA and nitrate; and (ii) if ATN measured by the untreated and extracted filters  
172 (i.e.,  $\text{ATN}_{\text{untreated}}$  and  $\text{ATN}_{\text{extracted}}$ ) were largely unchanged, loss of EC should be negligible. In the  
173 following discussions,  $\Delta\text{ATN}$ , which is defined as  $\text{ATN}_{\text{extracted}} - \text{ATN}_{\text{untreated}}$ , will be introduced to  
174 quantify the extraction-induced changes of ATN.

175 In the 2018–2019 campaign,  $\Delta\text{ATN}$  were close to zero for some of the samples, whereas for  
176 the remaining ones, ATN typically decreased to varying degrees after the extraction (Figure 1a).  
177 Here we noticed two distinct samples when exploring the  $\Delta\text{ATN}$  results (circled in Figure 1a). One  
178 of them showed the most significant decrease of ATN after extraction (with a  $\Delta\text{ATN}$  of  $-0.32$ ) during  
179 the 2018–2019 measurement period, whereas  $\Delta\text{ATN}$  was also considerable for the other sample ( $-$   
180  $0.25$ ). The two distinct samples were collected successively during January 12–14, 2019. In this  
181 period, relative humidity (RH) stayed above 85%, and both the sulfur oxidation ratio (SOR) and the  
182 nitrogen oxidation ratio (NOR) exceeded 0.2, with record high concentrations of sulfate ( $\sim 30 \mu\text{g}/\text{m}^3$ )  
183 and nitrate ( $\sim 40 \mu\text{g}/\text{m}^3$ ) for the 2018–2019 winter. Given the enhanced production of secondary  
184 inorganic aerosols, removal of nitrate by the extraction was a likely cause for the negative  $\Delta\text{ATN}$  of  
185 the two distinct samples. Sulfate was not considered here, since it is insoluble in methanol. As  
186 another component that could result in negative  $\Delta\text{ATN}$ , SOA could not be directly measured,  
187 whereas the indirect estimating approaches such as the EC-tracer method typically required EC  
188 concentration. We did not predict SOA at this stage, since the EC measurement uncertainties (e.g.,

189 the loss of EC during extraction) had not been comprehensively evaluated. However, similar to SOA,  
 190 formation of sulfate and nitrate was contributed by both heterogeneous and gas-phase reactions (Liu  
 191 et al., 2021; Wang et al., 2023), indicating that it should be acceptable to reflect the production of  
 192 secondary aerosols (including SOA) based on a synthesis of SOR and NOR. In other words, it was  
 193 very likely that the atmospheric conditions with elevated SOR and NOR (e.g., January 12–14, 2019)  
 194 were also favorable for SOA formation (this inference would be validated in Section 3.3). For the  
 195 two distinct samples, therefore, the removal of scattering components, including not only nitrate but  
 196 also SOA, was inferred to be highly responsible for the considerable extraction-induced decreases  
 197 of ATN.

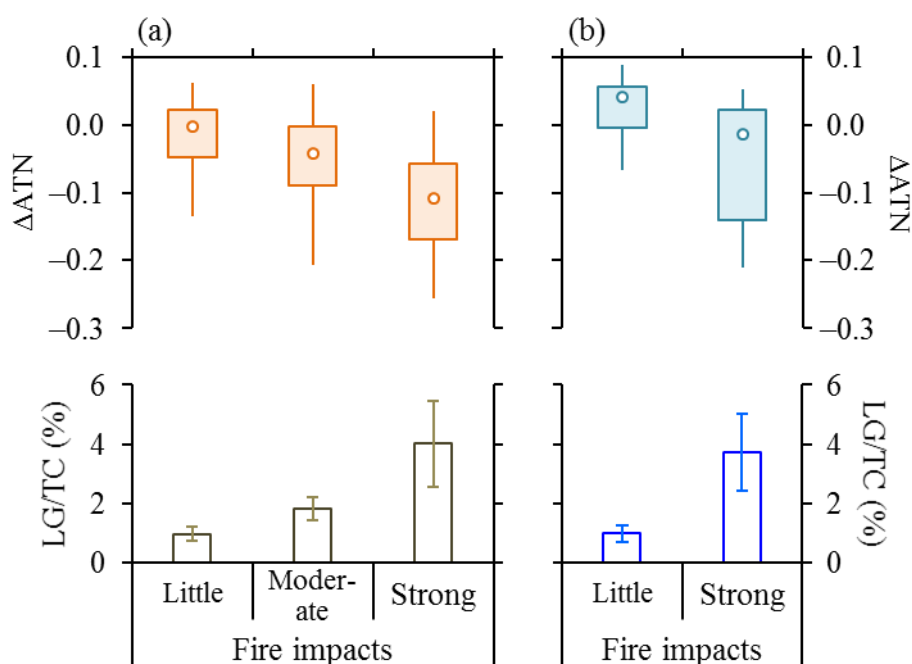


198

199 **Figure 1.** (a) Dependence of  $\Delta\text{ATN}$ , i.e.,  $\text{ATN}_{\text{extracted}} - \text{ATN}_{\text{untreated}}$ , on RH during the 2018–2019  
200 campaign, with results in different SOR + NOR ranges distinguished. The dashed line indicates a  
201  $\Delta\text{ATN}$  of zero. The dashed oval highlights two samples characterized by high RH levels, enhanced  
202 formation of secondary aerosols, and considerable decreases of ATN after extraction. (b)  
203 Comparisons of  $\Delta\text{ATN}$  (upper panel) and SOR + NOR (lower panel) across different RH ranges  
204 (i.e., below 60%, 60–70%, 70–80% and above 80% as indicated by A–D, respectively) during the  
205 2019–2020 campaign. To isolate the role of RH, only the samples with little influence of agricultural  
206 fires were involved in the comparison. In each panel, lower and upper box bounds indicate the 25th  
207 and 75th percentiles, the whiskers below and above the box indicate the 5th and 95th percentiles,  
208 and the open circle within the box marks the median (the same hereinafter). (c) The same as (b) but  
209 for 2020–2021.

210       Regarding the entire 2018–2019 campaign, humid events were actually uncommon, and most  
211 samples with negative  $\Delta\text{ATN}$  values concentrated in the conditions with relatively low RH levels of  
212 below 80 % (Figure 1a). Thus, in addition to the enhanced secondary aerosol production at high RH,  
213 there must exist other influencing factors responsible for the change of ATN for the 2018–2019  
214 samples. We then investigated the role of biomass burning, which could emit strongly-absorbing  
215 BrC with mass absorption efficiencies comparable to black carbon (Alexander et al., 2008; Hoffer  
216 et al., 2016; McClure et al., 2020). The 2018–2019 campaign was characterized by frequent  
217 occurrences of agricultural fires (Figure S1), mainly in winter due to a one-off policy which crudely  
218 approved a three-month long period (early December 2018 to early March 2019) for legitimate open  
219 burning. In our previous studies (Cheng et al., 2021a), the fire episodes were identified by the  
220 measured levoglucosan to organic carbon ratios ( $\text{LG}/\text{OC}^*$ , where  $\text{OC}^*$  indicates the untreated OC  
221 based on IMPROVE-A) together with the satellite-based fire hotspots, and the 2018–2019 samples  
222 were classified into three groups with increasing impacts of open burning. In this study, we revisited  
223 the classifications using the levoglucosan to TC ratios ( $\text{LG}/\text{TC}$ ), as the TC measurement was  
224 independent of thermal-optical protocol. The classifications made by Cheng et al. (2021a) were  
225 found to still hold, as  $\text{LG}/\text{TC}$  correlated strongly with  $\text{LG}/\text{OC}^*$  ( $r = 0.998$ ; Figure S2). As shown in

226 Figure 2a,  $\Delta$ ATN were close to zero (with a median value of 0.00) under little impact of open  
 227 burning. However,  $\Delta$ ATN turned negative when the fire impacts were non-negligible, and the  
 228 negative  $\Delta$ ATN values became more considerable as the fire impacts increased. For the 2018–2019  
 229 campaign, therefore, the occurrences of negative  $\Delta$ ATN were strongly associated with agricultural  
 230 fires, e.g., through the removal of BrC by extraction. In addition, both nitrate and NOR were found  
 231 to increase with stronger influences of agricultural fires (Figure S3), presumably due to the  
 232 enhancement of nitrate production by open burning emissions (Akagi et al., 2012; Collier et al.,  
 233 2016; Liu et al., 2016b). Thus, although the nitrate concentrations (Figure S3) were the lowest for  
 234 2018–2019 among the three campaigns, the removal of nitrate by extraction could also be partially  
 235 responsible for the association between  $\Delta$ ATN and agricultural fires.



236  
 237 **Figure 2.** (a) Comparisons of  $\Delta$ ATN (upper panel) and LG/TC (on a basis of carbon mass; lower  
 238 panel) across three cases with increasing impacts of agricultural fires during the 2018–2019  
 239 campaign. To highlight the role of fires, the two distinct samples showing apparent influences of  
 240 RH (as circled in Figure 1a) were not involved in the comparisons. (b) Comparisons of  $\Delta$ ATN (upper  
 241 panel) and LG/TC (lower panel) between two cases with little and strong impacts of agricultural  
 242 fires during the 2020–2021 campaign. Only the samples with RH levels of below 70% were  
 243 involved, because (i) the influence of RH was insignificant for this RH range and (ii) the majority

244 of the 2020–2021 samples with strong fire impacts (24 out of 27) fell within this RH range. The  
245 “moderate” case was not identified for 2020–2021. This is mainly because in response to different  
246 policies on open burning, the agricultural fires spanned a relatively long period (more than two  
247 months) during 2018–2019 but concentrated in April during 2020–2021 (Cheng et al., 2022).

248 Figures 1a and 2a suggest that ATN indeed decreased after the extraction for some of the 2018–  
249 2019 samples. However, the negative  $\Delta$ ATN were found to be associated typically with agricultural  
250 fires and occasionally with high RH conditions. The underlying mechanisms could be attributed  
251 primarily to the removal of BrC and scattering components (including SOA and nitrate), respectively.  
252 Importantly,  $\Delta$ ATN were negligible after excluding these two distinct cases (Figure 2a), suggesting  
253 that the loss of insoluble carbon (e.g., EC) should be minimal during our extraction procedures.

254 In addition to the two distinct samples shown in Figure 1a, the connections between  $\Delta$ ATN and  
255 RH could be further confirmed by the 2019–2020 campaign, which experienced much more high-  
256 RH events (mainly in winter) compared to 2018–2019 (Figure S4). As shown in Figure 1b for the  
257 2019–2020 samples with little impact of agricultural fires, the high-RH samples were characterized  
258 by elevated SOR and NOR, pointing to enhanced formation of secondary aerosols (presumably  
259 including SOA). A clear association was also observed between  $\Delta$ ATN and RH.  $\Delta$ ATN were  
260 typically negligible when RH stayed below 70%, showing median  $\Delta$ ATN values of 0.00 and –0.01  
261 for the RH ranges of below 60% and 60–70%, respectively. However,  $\Delta$ ATN deviated more  
262 significantly from zero when RH further increased, e.g., with a median  $\Delta$ ATN value of –0.28 for the  
263 RH range of above 80%. Although some primary organic compounds could also be non-absorbing  
264 at 632 nm, it is unlikely that the abundances or emissions of such species would depend on RH.  
265 Thus, the most possible explanation for the negative  $\Delta$ ATN observed at relatively high RH levels  
266 should be the removal of secondary components (including SOA and nitrate) by extraction.

267 The 2019–2020 campaign covered a shorter period (Table 1) and encountered much fewer fire

268 episodes ( $N = 2$ ) compared to 2018–2019 and 2019–2020 ( $N = 21$  and  $27$ , respectively). The two  
269 2019–2020 samples with strong fire impacts had similar RH levels of  $\sim 50\%$  and only one of them  
270 exhibited considerable  $\Delta\text{ATN}$  ( $-0.26$ ; Figure S5), which could be attributed to the removal of BrC  
271 by extraction. For the 2019–2020 campaign, therefore, the extraction-induced decreases of ATN  
272 were caused primarily by the removal of scattering components. In addition, as shown in Figure 1b,  
273 the close-to-zero  $\Delta\text{ATN}$  values observed at the relatively low RH levels (e.g., with a median  $\Delta\text{ATN}$   
274 of  $0.00$  for the RH range of below  $60\%$ ) further supported the inference on negligible loss of  
275 insoluble carbon during extraction.

276 The 2020–2021 campaign experienced more high-RH events compared to 2018–2019 and  
277 more agricultural-fire episodes than 2019–2020 (Figure S1). Correspondingly, the extraction-  
278 induced changes of ATN could be attributed to the removal of either scattering components (Figure  
279 1c) or BrC (Figure 2b). Similar to results from the other two campaigns,  $\Delta\text{ATN}$  were close to zero  
280 for the 2020–2021 periods with low RH levels and little impact of open burning (Figure 1c),  
281 demonstrating again that the extraction-induced loss of insoluble carbon was negligible.

282 The discussions above suggested that it was acceptable to attribute the reduced TC  
283 concentrations in the extracted punches to the dissolving of organic compounds. This in turn  
284 supported the determination of MSOC as the difference in TC between the untreated and extracted  
285 punches, i.e.,  $\text{TC}_{\text{untreated}} - \text{TC}_{\text{extracted}}$ . TC was used here since it was independent of analytical method,  
286 i.e., not influenced by the uncertainties in the split of OC and EC. In addition, both  $\text{TC}_{\text{untreated}}$  and  
287  $\text{TC}_{\text{extracted}}$  had been corrected by blanks before being used to calculate MSOC. A total of 53 filters  
288 were kept as blanks for the three campaigns. The blank TC decreased slightly after the extraction  
289 (from  $0.61 \pm 0.23$  to  $0.44 \pm 0.21 \mu\text{gC}/\text{cm}^3$ ), with no EC detected for either the untreated or extracted

290 filters. A possible explanation for the decrease was the dissolving of organic compounds, which  
291 constituted the TC of the untreated blank filters, into the solvent. Importantly, the absence of  
292 extraction-induced increase in blank TC indicated that the methanol retained by the filters after the  
293 extraction could be completely volatilized during the drying process, and consequently would not  
294 influence the split of OC and EC for the extracted samples.

### 295 **3.2 Evaluation of EC from different methods**

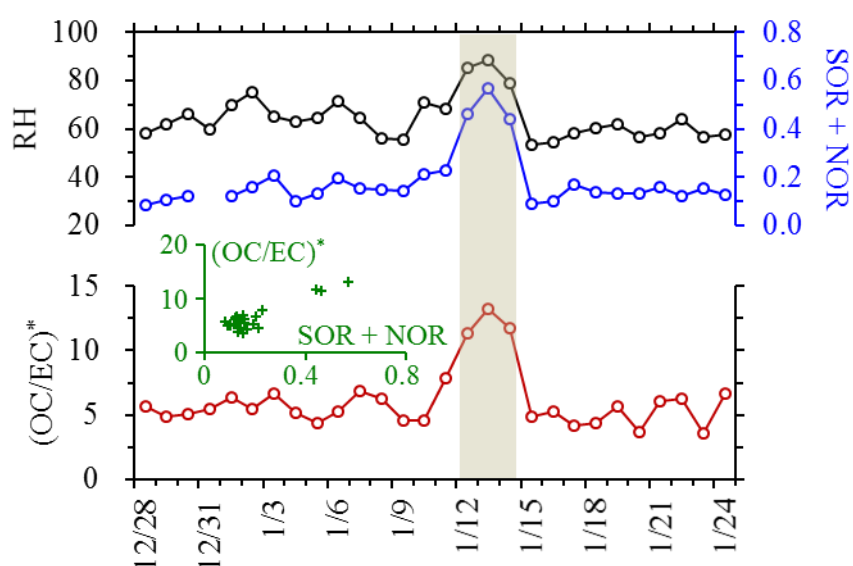
296 As mentioned in Section 2.1, all the pairs of untreated and extracted punches were measured  
297 by IMPROVE-A, with selected pairs also analyzed by NIOSH. A major purpose of involving  
298 NIOSH was to unfold the EC discrepancies between different protocols, an important indicator for  
299 the EC measurement uncertainties. The 2018–2019 campaign was characterized by intensive  
300 agricultural fires in winter (Figure S1), providing an opportunity to evaluate the effects of open  
301 burning emissions on EC determination. In addition, considering this campaign was the first one to  
302 investigate EC measurement uncertainties in Northeast China, all the 2018–2019 samples were  
303 analyzed by NIOSH (Table 1). The 2019–2020 campaign was characterized by unusually high levels  
304 of RH in winter (Figure S1), which were expected to favor heterogeneous chemistry. To investigate  
305 the influences of secondary aerosols on EC determination, NIOSH was applied to all the samples  
306 collected in December 2019 and January 2020. The 2020–2021 campaign showed mixed features  
307 of the other two campaigns, i.e., high RH events and agricultural fire episodes in January and April  
308 of 2021, respectively (Figure S1). Thus all the samples from these two months were analyzed by  
309 NIOSH. For the other periods of 2019–2020 and 2020–2021, NIOSH was used every five samples.  
310 As shown in Table 1, a total of 339 pairs of untreated and extracted punches were analyzed by  
311 NIOSH in addition to IMPROVE-A. Then for the majority of the Harbin samples (339 out of 486),

312 there were four sets of EC and OC results. Two sets were derived from the untreated punch, using  
313 the IMPROVE-A and NIOSH protocols, respectively. For the third set, EC was measured by the  
314 extracted punch based on IMPROVE-A ( $EC_{\text{extracted, IMPROVE-A}}$ ) while OC was calculated as the  
315 difference between  $TC_{\text{untreated}}$  and  $EC_{\text{extracted, IMPROVE-A}}$ . OC and EC of the fourth set were defined  
316 similarly based on NIOSH. The following patterns were observed when comparing the EC and OC  
317 results across different methods.

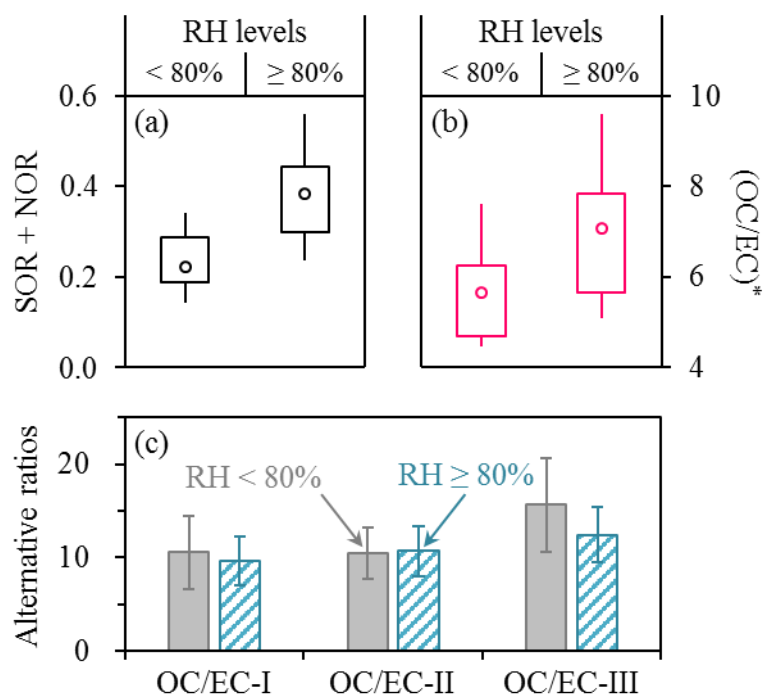
318 First, only the OC to EC ratios determined by the untreated samples using IMPROVE-A, i.e.,  
319  $(OC/EC)^*$ , could properly reflect secondary aerosol formation. For a typical urban site,  
320 anthropogenic emissions such as those from coal combustion and vehicles were usually considered  
321 relatively stable during a given period, e.g., a specific season. Then the temporal variations of  
322 OC/EC could be used to track SOA formation (e.g., as done by the EC-tracer method), after  
323 excluding the episodes impacted by irregular emissions such as open burning and fireworks. As  
324 firework events were not involved in this study, here we focused on three periods owing all the four  
325 sets of OC and EC results with insignificant influence of agricultural fires, i.e., a four-week long  
326 period in the 2018–2019 winter (December 28, 2018–January 25, 2019), December 2019 to January  
327 2020, and January 2021. In the first case, three samples collected during January 12–15, 2019  
328 exhibited persistently high levels of RH, SOR and NOR (Figure 3), pointing to enhanced formation  
329 of secondary species possibly through heterogeneous chemistry. This humid period was supposed  
330 to favor SOA production as well, since field observational results from the North China Plain  
331 repeatedly showed concurrent increases of secondary inorganic and organic components under high  
332 RH conditions in winter (Hu et al., 2016b; Liu et al., 2020; Sun et al., 2020). Similar to SOR and  
333 NOR,  $(OC/EC)^*$  also increased substantially for the humid period during January 12–15, 2019



334 (averaging  $12.09 \pm 0.97$ ) compared to results from the other samples (averaging  $5.39 \pm 1.04$ ; Figure  
 335 3). However, unlike  $(OC/EC)^*$ , OC to EC ratios determined in other approaches (namely OC/EC-I,  
 336 -II and -III) less accurately or failed to track the RH-dependent enhancement of SOA formation  
 337 (Figure S6). This conclusion also held for the other winters. Briefly,  $(OC/EC)^*$  increased  
 338 concurrently with SOR and NOR at high RH levels for the winters of both 2019–2020 (Figure 4)  
 339 and 2020–2021 (Figure S7), whereas the alternative OC/EC ratios did not.



340  
 341 **Figure 3.** Temporal variations of RH, SOR +NOR (upper panel) and  $(OC/EC)^*$  (lower panel) during  
 342 the 2018–2019 winter period with insignificant impact of agricultural fires. The shadowed area  
 343 highlights three distinct samples characterized by high RH and enhanced formation of secondary  
 344 aerosols. The inner scatter plot shows the positive dependence of  $(OC/EC)^*$  on SOR + NOR ( $r =$   
 345 0.89).



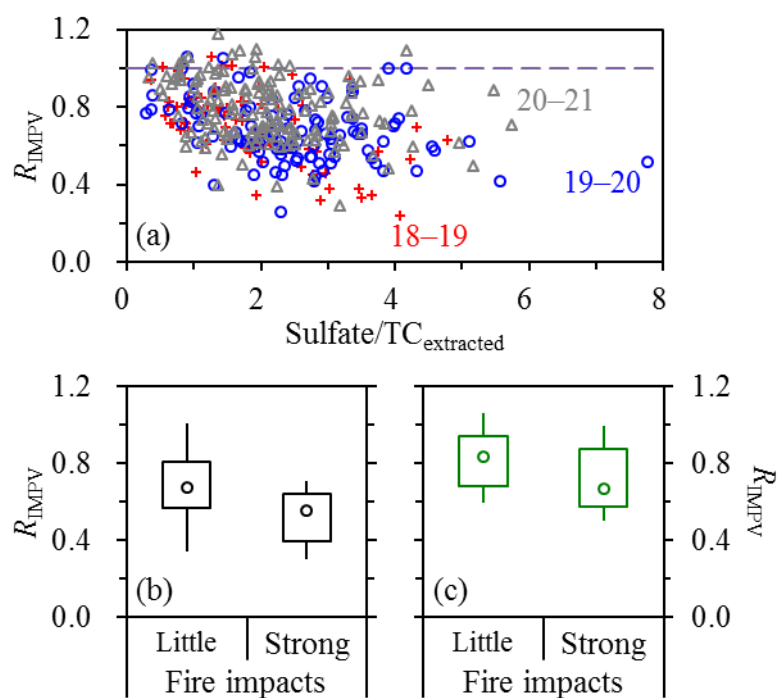
346

347 **Figure 4.** Comparisons of (a) SOR + NOR, (b)  $(OC/EC)^*$  and (c) alternative OC/EC ratios between  
 348 RH ranges of below and above 80%, based on results from December 2019–January 2020. In (c),  
 349 OC/EC-I was derived from OC and EC measured by the untreated sample using NIOSH. OC/EC-II  
 350 was calculated by  $EC_{\text{extracted, IMPROVE-A}}$  and the corresponding OC (i.e.,  $TC_{\text{untreated}} - EC_{\text{extracted, IMPROVE-A}}$ ). OC/EC-III  
 351 was determined similarly based on NIOSH.

352 Second, EC measured by the extracted filters ( $EC_{\text{extracted}}$ ) were typically lower than results from  
 353 the untreated ones ( $EC_{\text{untreated}}$ ), especially for IMPROVE-A. This pattern should be attributed  
 354 primarily to EC measurement uncertainties rather than EC loss during the extraction, as the later  
 355 had been demonstrated to be negligible in Section 3.1. Two influencing factors were identified for  
 356 the  $EC_{\text{extracted}}$  to  $EC_{\text{untreated}}$  ratios based on IMPROVE-A (defined as  $R_{\text{IMPV}}$ ). The first one was the  
 357 relative abundance of sulfate on the extracted filter, which could be estimated by the sulfate to  
 358  $TC_{\text{extracted}}$  ratio ( $\text{sulfate}/TC_{\text{extracted}}$ ). For the samples with little impact of open burning,  $R_{\text{IMPV}}$  tended  
 359 to decrease as  $\text{sulfate}/TC_{\text{extracted}}$  became higher, with generally consistent relationships for the three  
 360 campaigns (Figure 5a). The median  $R_{\text{IMPV}}$  was 0.86 when the  $\text{sulfate}/TC_{\text{extracted}}$  ratios were below 1,  
 361 and decreased to 0.62 for the  $\text{sulfate}/TC_{\text{extracted}}$  range of above 4 (Figure S8). We proposed the  
 362 following hypotheses for the negative dependence of  $R_{\text{IMPV}}$  on  $\text{sulfate}/TC_{\text{extracted}}$ . We first simplified

363 the remained particles on the extracted filters as a mixture of EC and sulfate, as nitrate and the vast  
364 majority of OC were soluble in methanol. Then a key assumption was that sulfate could promote  
365 the transmission of laser light through the extracted filters (e.g., by forward scattering; Petzold et  
366 al., 2005), indicating that the volatilization of sulfate during the inert mode of thermal-optical  
367 analysis could lead to a decrease of the transmittance signal ( $I$ ). Thus in the oxidizing mode, a  
368 fraction of EC would be consumed to compensate this decrease (i.e. make  $I$  return to its initial value)  
369 and consequently, elemental carbon mass would be underestimated by  $EC_{\text{extracted}}$ .

370 In addition to sulfate/ $TC_{\text{extracted}}$ , another influencing factor for  $R_{\text{IMPV}}$  was open burning.  $R_{\text{IMPV}}$   
371 determined for the agricultural-fire episodes were lower compared to results from the periods with  
372 the same sulfate/ $TC_{\text{extracted}}$  range but little impact of open burning (Figures 5b and 5c). As discussed  
373 in Section 3.1, agricultural fires could be a source for strongly-absorbing BrC. For the untreated  
374 filters, such BrC could be difficult to be properly distinguished from EC by the carbon analyzer used  
375 in this study. Thus, a possible explanation for the reduced  $R_{\text{IMPV}}$  under strong impacts of agricultural  
376 fires was that open burning emissions could result in overestimation of elemental carbon mass by  
377  $EC_{\text{untreated}}$  (i.e., the positive artifact). Under this assumption, the fire-induced decreases of  $R_{\text{IMPV}}$   
378 could be translated into positive artifacts of ~25% (based on the median  $R_{\text{IMPV}}$  determined under  
379 little and strong fire impacts) for the open burning episodes of 2018–2019 and 2020–2021.



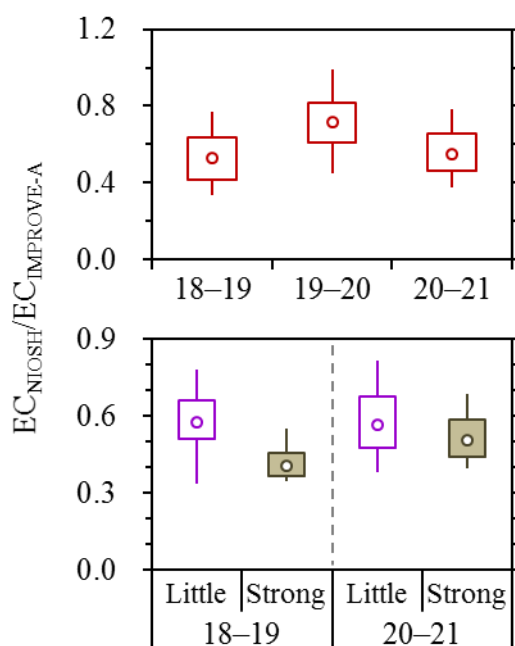
380

381 **Figure 5.** (a) Dependence of  $R_{\text{IMPVS}}$  (i.e., the  $\text{EC}_{\text{extracted}}$  to  $\text{EC}_{\text{untreated}}$  ratio based on IMPROVE-A) on  
 382 sulfate/ $\text{TC}_{\text{extracted}}$ , with results from different campaigns shown separately. Only the samples with  
 383 little influence of open burning were involved. (b) Comparison of  $R_{\text{IMPVS}}$  between the 2018–2019  
 384 samples with strong impacts of agricultural fires (as indicated by “Strong”) and those with the same  
 385 sulfate/ $\text{TC}_{\text{extracted}}$  range but little fire impact (as indicated by “Little”). (c) The same as (b) but for  
 386 2020–2021.

387 Similar to  $R_{\text{IMPVS}}$ , the  $\text{EC}_{\text{extracted}}$  to  $\text{EC}_{\text{untreated}}$  ratios based on NIOSH ( $R_{\text{NIOSH}}$ ) also tended to  
 388 decrease with increasing sulfate/ $\text{TC}_{\text{extracted}}$ , e.g., with the median  $R_{\text{NIOSH}}$  decreasing from 1.00 to  
 389 0.78 as sulfate/ $\text{TC}_{\text{extracted}}$  became higher (Figure S8). Thus, the inference on the underestimation of  
 390 elemental carbon mass by  $\text{EC}_{\text{extracted}}$  should be valid for NIOSH as well. The close-to-one  $R_{\text{NIOSH}}$   
 391 but lower  $R_{\text{IMPVS}}$  (0.86) determined for the same sulfate/ $\text{TC}_{\text{extracted}}$  range of below 1 (Figure S8)  
 392 suggested that the extraction led to comparable  $\text{EC}_{\text{untreated}}$  and  $\text{EC}_{\text{extracted}}$  when using NIOSH but  
 393 resulted in relatively low  $\text{EC}_{\text{extracted}}$  when using IMPROVE-A. This prohibited the use of  $\text{EC}_{\text{untreated}}$   
 394 vs.  $\text{EC}_{\text{extracted}}$  relationship for the assessment of EC loss during extraction, and highlighted the  
 395 significance of the  $\Delta\text{ATN}$ -based evaluation results in Section 3.1. It is also noteworthy that for  
 396 NIOSH, ~40% of the samples showed  $R_{\text{NIOSH}}$  values above 1, indicating that their  $\text{EC}_{\text{untreated}}$  were

397 even lower than  $EC_{\text{extracted}}$ . A possible explanation was that when using NIOSH,  $EC_{\text{untreated}}$  frequently  
398 underestimated the elemental carbon mass, and the underestimation could be more significant than  
399 that by  $EC_{\text{extracted}}$ . In addition, no evidence was observed for apparent influence of open burning on  
400  $R_{\text{NIOSH}}$  (Figure S9). It appeared that the determination of  $EC_{\text{untreated}}$  was less significantly affected  
401 by agricultural fires when using NIOSH compared to IMPROVE-A.

402 The third pattern derived from the comparison of EC results across different methods was that  
403 for the untreated samples, the IMPROVE-A protocol led to higher EC values than NIOSH (Figure  
404 6). This pattern was in line with results from other regions (e.g., Chow et al., 2004; Piazzalunga et  
405 al., 2011; Giannoni et al., 2016), and was consistent with the previous inference on the uncertainty  
406 of the NIOSH-based  $EC_{\text{untreated}}$ . In addition, the discrepancies between  $EC_{\text{untreated}}$  measured by the  
407 two protocols became larger with increasing impacts of agricultural fires (Figure 6). This trend could  
408 be attributed to the open-burning-induced overestimation of elemental carbon mass by  $EC_{\text{untreated}}$   
409 (i.e., the positive artifact), which was considerable for IMPROVE-A (Figures 5b and 5c) but  
410 appeared insignificant when using NIOSH (Figure S9). Another noteworthy feature in Figure 6 was  
411 that compared to the open burning episodes of 2020–2021, the 2018–2019 fire events showed more  
412 significant inter-protocol differences in  $EC_{\text{untreated}}$ . The contrast appeared to indicate that the 2018–  
413 2019 fires, which were inferred to have lower combustion efficiencies (Cheng et al., 2022), could  
414 result in more significant positive artifacts for IMPROVE-A.



415

416 **Figure 6.** Ratios between EC measured by different protocols using the untreated samples, i.e.,  
 417  $EC_{\text{NIOSH}}/EC_{\text{IMPROVE-A}}$ . The upper panel compares the ratios across campaigns. The lower panel  
 418 compares the ratios between the samples with little and strong impacts of agricultural fires, with  
 419 results from 2018–2019 and 2020–2021 shown separately.

420 As reflected by the discussions above, all the EC results had uncertainties, regardless of the  
 421 pretreatment approaches (with or without methanol extraction) and temperature protocols  
 422 (IMPROVE-A or NIOSH). For the untreated samples, the IMPROVE-A protocol led to OC/EC  
 423 ratios in reasonable accordance with secondary aerosol formation, whereas NIOSH did not.  
 424 However, it must be acknowledged that for IMPROVE-A, the elemental carbon mass was likely  
 425 overestimated by  $EC_{\text{untreated}}$  under strong impacts of agricultural fires (by ~25%), presumably due to  
 426 the interference of BrC. Although this positive artifact could in principle be reduced or minimized  
 427 by methanol extraction, a new issue arose that the elemental carbon mass was underestimated by  
 428  $EC_{\text{extracted}}$  (i.e., the negative artifact), which was inferred to be associated with the volatilization of  
 429 sulfate from the extracted samples during the inert mode of thermal-optical analysis. The  
 430 significance of the negative artifact could be reflected by decreases of EC after extraction, which  
 431 were as high as ~15–40% for IMPROVE-A (Figure S8). Importantly, the negative artifact was not

432 limited to the open-burning-impacted samples, i.e., it also biased the measurement of samples with  
433 little influence of agricultural fires. Thus, although the methanol extraction could reduce the positive  
434 artifacts of  $EC_{\text{untreated}}$  for the fire episodes, it in turn caused more significant negative artifacts of  
435  $EC_{\text{extracted}}$  for all the Harbin samples. Consequently, the methanol extraction was not considered an  
436 effective approach to improve the measurement of elemental carbon mass in this study. In the  
437 following discussions, the  $EC_{\text{untreated}}$  results based on IMPROVE-A, i.e.,  $EC^*$ , will be used for  
438 exploring the sources of light-absorbing carbon in Harbin.

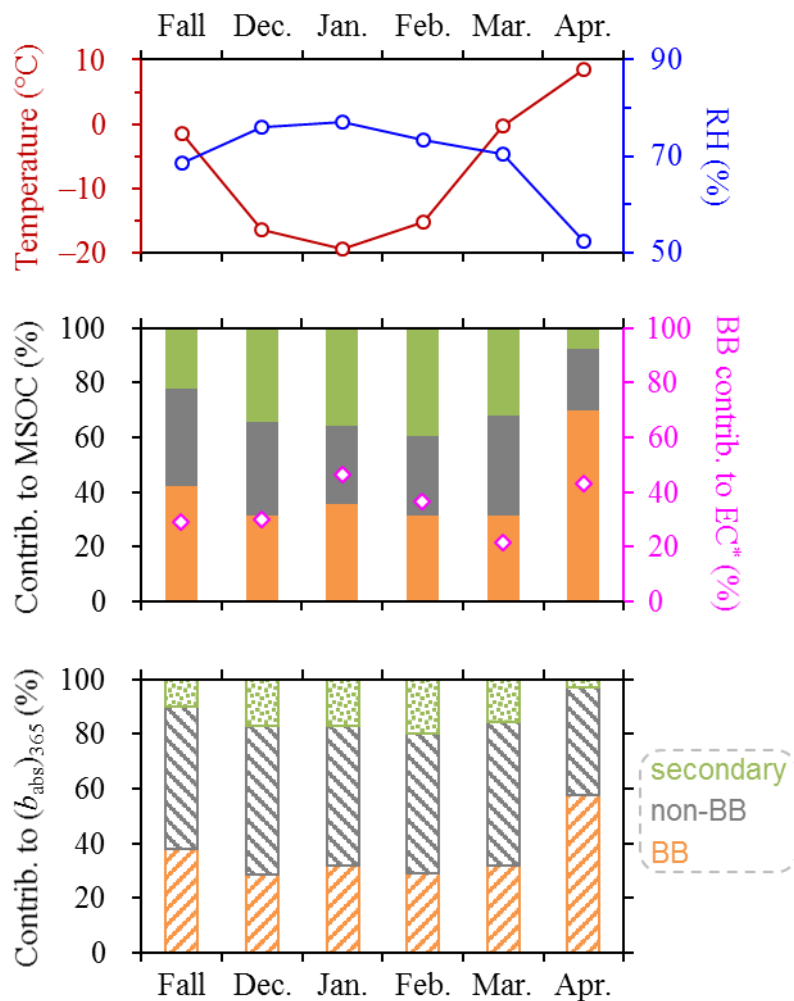
### 439 **3.3 Sources of light-absorbing carbon**

440 Based on the observational results, EPA's Positive Matrix Factorization (PMF) model (version  
441 5.0) was used to elucidate the sources of light-absorbing carbonaceous aerosols. Here we focus on  
442 the 2020–2021 campaign, which experienced coexisted features of 2018–2019 and 2019–2020 (i.e.,  
443 strong impacts of agricultural fires and high-RH conditions, respectively). A six-factor solution was  
444 resolved by PMF (Figure S10), using time series of  $EC^*$ , BrC mass concentration (i.e., MSOC),  
445 light absorption coefficient of BrC at 365 nm [i.e.,  $(b_{\text{abs}})_{365}$ ], levoglucosan, chloride, sulfate, nitrate  
446 and ammonium as inputs. Briefly, two factors were considered secondary due to their dominant  
447 contributions to secondary inorganic ions; two factors were attributed to primary emissions from  
448 biomass burning (BB), as they explained the vast majority of levoglucosan; the last two factors were  
449 important contributors to EC and chloride but had little levoglucosan or secondary species, pointing  
450 to primary emissions from non-BB sources (e.g., coal combustion and vehicles). MSOC apportioned  
451 into these three source categories were termed as sec-MSOC, pri-MSOC<sub>BB</sub> and pri-MSOC<sub>non-BB</sub>,  
452 respectively. Source-resolved BrC light absorption were defined similarly, as sec-BrC, pri-BrC<sub>BB</sub>  
453 and pri-BrC<sub>non-BB</sub>.  $EC^*$  emitted by the BB and non-BB sources were referred to as  $EC_{\text{BB}}$  and  $EC_{\text{non-}}$

454 BB, respectively. Figure 7 presents an overview of the source apportionment results. The temporal  
455 variations of the MSOC and  $(b_{\text{abs}})_{365}$  source attributions were characterized by considerable  
456 increases of the BB contribution in April, the season with frequent occurrences of agricultural fires.  
457 It was also noticed that secondary formation was an important source of MSOC (especially in winter)  
458 but contributed less significantly to  $(b_{\text{abs}})_{365}$ . This pattern could be attributed to the fact that  
459 secondary BrC was typically less absorbing than primary BrC (Kumar et al., 2018; Cappa et al.,  
460 2020). For the sources of  $\text{EC}^*$ , a noteworthy feature was that the BB contributions reached similarly  
461 higher levels in the fire-impacted April and January, the coldest month with little influence of open  
462 burning.

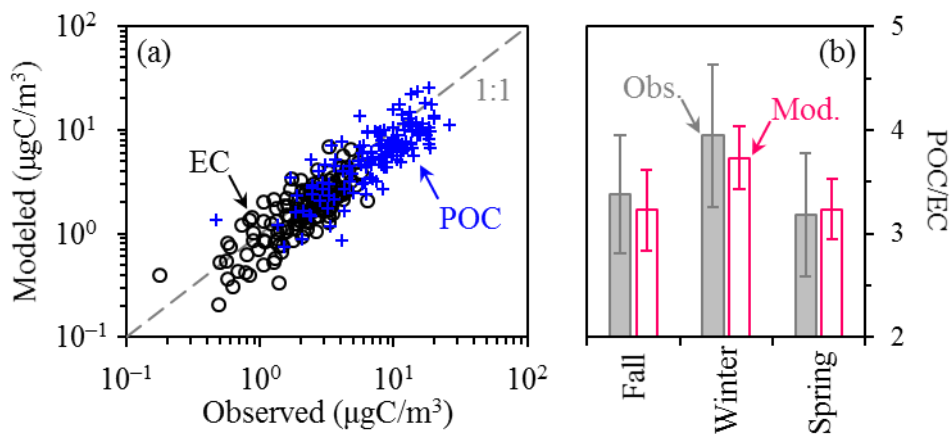
463 The revised CMAQ predicted the concentrations of organic and elemental carbon (i.e.,  $\text{OC}_{\text{mod}}$   
464 and  $\text{EC}_{\text{mod}}$ ), with the primary and secondary OC (i.e.,  $\text{POC}_{\text{mod}}$  and  $\text{SOC}_{\text{mod}}$ ) results also available.  
465 Given that MSOC approximately equaled  $\text{OC}^*$  (Figure S11), it should be acceptable to perform  
466 direct comparisons between these two terms from various sources, i.e., between  $\text{SOC}_{\text{mod}}$  and sec-  
467 MSOC, and between  $\text{POC}_{\text{mod}}$  and primary MSOC (pri-MSOC, calculated as the sum of  $\text{pri-MSOC}_{\text{BB}}$   
468 and  $\text{pri-MSOC}_{\text{non-BB}}$ ). For the samples with little influence of agricultural fires, the revised CMAQ  
469 generally reproduced the observation-based pri-MSOC and  $\text{EC}^*$  (Figure 8a), with mean biases of –  
470  $1.94 \mu\text{gC}/\text{m}^3$  ( $\text{POC}_{\text{mod}} - \text{pri-MSOC}$ ) and  $-0.43 \mu\text{gC}/\text{m}^3$  ( $\text{EC}_{\text{mod}} - \text{EC}^*$ ), respectively. In this case, the  
471  $\text{POC}_{\text{mod}}$  to  $\text{EC}_{\text{mod}}$  ratios also coincided with the measurement results, i.e., the pri-MSOC to  $\text{EC}^*$   
472 ratios. For example, the two ratios agreed with respect to both the absolute values and seasonal  
473 variations (Figure 8b). These consistencies to some extent supported the reliability of the source  
474 apportionment results from PMF.





475

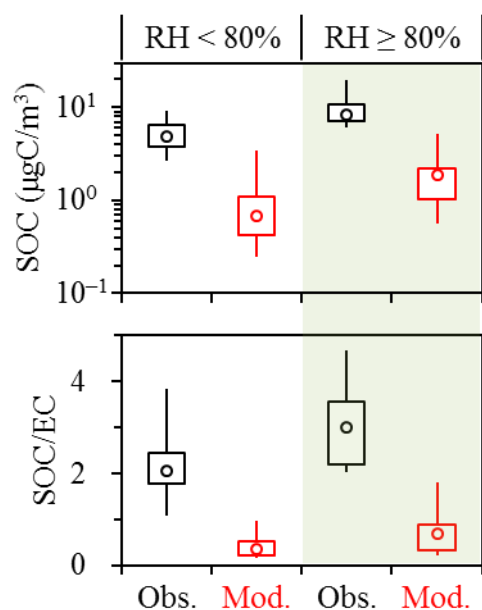
476 **Figure 7.** Monthly-averaged temperatures and RH (upper panel), and source apportionment results  
 477 of MSOC, EC (middle panel) and  $(b_{\text{abs}})_{365}$  (lower panel) for the 2020–2021 campaign. Fall indicates  
 478 mid-October to November. In the middle and lower panels, sources of MSOC and  $(b_{\text{abs}})_{365}$  were  
 479 classified into three categories distinguished by different colors in the bar charts, i.e., primary BB  
 480 emissions in orange, primary non-BB emissions in grey and secondary in green. Sources of EC\*  
 481 were separated into BB and non-BB emissions, with the BB contributions shown by the diamonds  
 482 in the middle panel.



483

484 **Figure 8.** Comparisons of the modeled and observed (a) POC and EC concentrations, and (b)  
485 seasonal POC to EC ratios for the 2020–2021 campaign. Only the samples with little fire impact  
486 were involved. The 1:1 line is also shown in (a).

487       The high-RH conditions were concentrated in the winter, i.e., December 2020 to February 2021.  
488 Such conditions were believed to favor SOA production, as indicated by the RH-dependent  
489 increases of SOR and NOR (Figures 1b and 1c). This inference was further confirmed by the PMF  
490 results, as both the sec-MSOC and sec-MSOC/EC\* were considerably enhanced after RH exceeding  
491 80% (Figure 9). The PMF results also confirmed the link between (OC/EC)\* and SOA formation,  
492 given the agreement between sec-MSOC and results from the EC-tracer method ( $r = 0.91$ ; Figure  
493 S12). The revised CMAQ predicted the RH-dependent enhancement of SOC formation as well.  
494 However, it failed to reproduce the observed SOC concentrations and SOC to EC ratios, with  
495 significant underestimations. For example, the modeling results only explained 18% and 22% of the  
496 observed SOC concentrations (corresponding to 19% and 26% of the observed SOC to EC ratios)  
497 for the RH ranges of below and above 80%, respectively. The results suggested that the SOA module  
498 of the revised CMAQ, including the newly-added heterogeneous mechanisms, still required  
499 substantial improvements. In addition, aerosol water could remain supercooled at the typical  
500 temperatures during winter in Harbin, which were down to about  $-25\text{ }^{\circ}\text{C}$  in terms of daily average  
501 (Rosenfeld and Woodley, 2000). For the frigid atmosphere in Northeast China, therefore,  
502 heterogeneous reactions in aerosol water were expected to prevail as long as RH reached sufficiently  
503 high levels. The mechanisms of low-temperature chemistry, which may differ from those in the  
504 relatively warm regions (e.g., Beijing), merit further investigations.

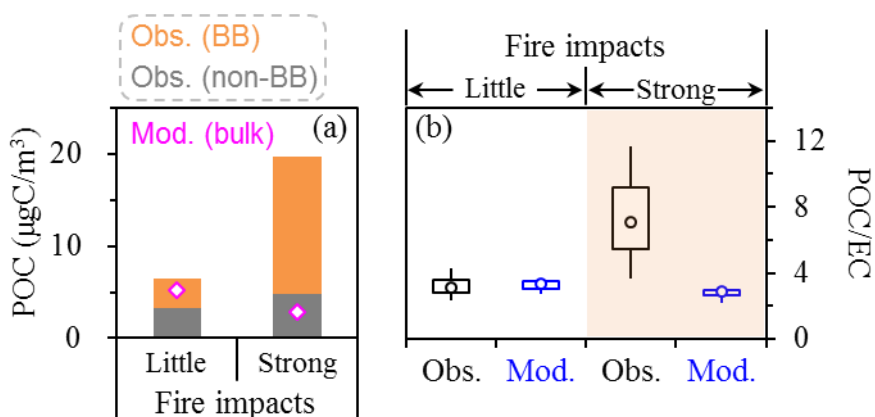


505

506 **Figure 9.** Comparisons of the modeled and observed SOC concentrations (upper panel) and SOC  
 507 to EC ratios (lower panel) for the 2020–2021 winter. The comparisons were performed for the RH  
 508 ranges of below and above 80% separately. Open burning impact was negligible for this period.

509 The agricultural fire episodes mainly occurred in April during the 2020–2021 measurement  
 510 period. PMF results suggested that the BB contributions to MSOC and EC\* increased significantly  
 511 for the fire episodes (reaching 72 and 44%, respectively) compared to other periods in spring (33  
 512 and 25%, respectively). The fire emissions also significantly increased the observation-based POC  
 513 concentrations (i.e., pri-MSOC) and POC to EC ratios (i.e., pri-MSOC/EC\*; Figure 10). This is  
 514 within expectation, since organic compounds were frequently found to constitute the vast majority  
 515 of the particulate emissions from open burning emissions (Hodgson et al., 2018; Garofalo et al.,  
 516 2019). Since the revised CMAQ did not predict biomass burning OC separately, comparison of the  
 517 modeling and observational results could only be made based on the bulk primary OC. As shown in  
 518 Figure 10, the model could not track the influences of agricultural fires on primary OC, e.g., as  
 519 indicated by the largely comparable  $\text{POC}_{\text{mod}}$  to  $\text{EC}_{\text{mod}}$  ratios between the fire episodes and other  
 520 periods in spring. It appeared that the fire emissions, which were derived from the FINN inventory,  
 521 were underestimated for the model simulation. In FINN, the open burning emissions were retrieved

522 using burned areas detected by the Terra and Aqua polar-orbiting satellites (Wiedinmyer et al., 2011).  
 523 A limitation of this approach was the missing of fires due to satellite overpass timing (Uranishi et  
 524 al., 2019), which was also the case for the Global Fire Emissions Database (GFED), another  
 525 commonly-used open burning inventory based on burned areas (Konovalov et al., 2018; Chen et al.,  
 526 2023). Previous studies suggested that the underestimation of open burning emissions by FINN or  
 527 GFED could be considerable, e.g., by a factor of as high as above 20 (Xie et al., 2024). Given the  
 528 massive agricultural sector in Harbin and surrounding areas (e.g., the Harbin-Changchun  
 529 metropolitan area), we suggest that the uncertainties of open burning inventories merit particular  
 530 attention for the modeling studies in this region.



531

532 **Figure 10.** Comparisons of the modeled and observed (a) POC concentrations and (b) POC to EC  
 533 ratios between the samples with little and strong fire impacts in the spring of 2021. In (a), the  
 534 observation-based results were shown by the bars (as the sum of BB and non-BB emissions), while  
 535 the modeling results were indicated by the diamonds.

536 It was also noticed that the mean bias in elemental carbon ( $\text{EC}_{\text{mod}} - \text{EC}^*$ ) was more significant  
 537 for the fire episodes ( $-1.26 \mu\text{gC}/\text{m}^3$ ) compared to other periods in spring ( $-0.44 \mu\text{gC}/\text{m}^3$ ). This  
 538 pattern could be attributed to two factors, including the underestimation of open burning emissions  
 539 by the inventory and the fire-associated overestimation of elemental carbon mass by  $\text{EC}^*$ . In other  
 540 words, both  $\text{EC}_{\text{mod}}$  and  $\text{EC}^*$  were subject to larger uncertainties for the fire episodes, resulting in

541 more significant model vs. observation discrepancies in elemental carbon concentration.

#### 542 **4. Conclusions and atmospheric implications**

543 Light-absorbing carbonaceous aerosols were investigated for Northeast China based on three  
544 campaigns conducted during 2018–2021 in Harbin. BrC masses were determined based on methanol  
545 extraction of filter samples, as the difference between TC concentrations of the untreated and  
546 extracted punches. A long-standing concern on this method was the loss of EC during extraction.  
547 This artifact was evaluated indirectly based on the extraction-induced changes of ATN, due to the  
548 lack of reference method for EC measurement. For different campaigns, it was repeatedly observed  
549 that ATN was largely unchanged after extraction, as long as the RH levels were unfavorable for  
550 secondary aerosol formation and the impacts of agricultural fires were negligible. This pointed to  
551 negligible loss of EC during extraction and consequently supported the robustness of the  
552 observational data on BrC mass. In addition, EC and OC concentrations were determined by four  
553 methods differing with respect to pretreatment approaches (with and without extraction of the filter  
554 samples) and thermal-optical protocols (IMPROVE-A and NIOSH). Results from the untreated  
555 samples using IMPROVE-A were found to provide OC to EC ratios in reasonable accordance with  
556 secondary aerosol formation. Thus EC determined by this method (EC\*) was used for the source  
557 apportionment of light-absorbing carbon, together with other input species such as BrC mass (i.e.,  
558 MSOC), BrC absorption coefficient and levoglucosan. In addition, the corresponding OC (OC\*)  
559 approximately equaled MSOC, the determination of which was laborious. This equivalence  
560 supported the simplification of MSOC as OC\* for further studies.

561 The observation-based source apportionment results showed increased contributions of  
562 secondary formation to BrC in winter, when the high-RH conditions concentrated. It was also

563 noticed that secondary formation contributed more significantly to BrC mass than BrC absorption,  
564 in line with the consensus that secondary BrC was typically less absorbing than primary BrC. In  
565 addition, agricultural fires were found to effectively enhance the BB contributions to BrC (in terms  
566 of either mass concentration or absorption coefficient) and EC.

567 The abundances and sources of OC and EC were also predicted by an air quality model with  
568 newly-added heterogeneous reactions. The general equivalence of BrC and OC masses supported  
569 direct comparisons of the observational and modeling results. The model properly reproduced POC  
570 and EC (in terms of both absolute concentration and POC to EC ratio) for the periods with little  
571 impact of agricultural fires. The model also predicted the existence of RH-dependent enhancement  
572 of SOC production in winter, but significantly underestimated the observed SOC concentrations.  
573 Another problem identified for the modeling results was the substantial underprediction of POC for  
574 the agricultural fire events, presumably due to underestimation of open burning emissions by the  
575 FINN inventory.

576 An agreement between observed and simulated results (e.g., with respect to aerosol abundances  
577 and sources) is essential for the development of efficient air pollution control strategies. In this study,  
578 we constrained the modeling results of carbonaceous aerosols by field observation, based on  
579 validated measurement results of BrC and EC. Two challenges were identified for the simulation of  
580 carbonaceous aerosols in Northeast China, i.e., significant underprediction of SOC and agricultural  
581 fire emissions. Our results suggest that the commonly-used CMAQ model requires substantial  
582 improvements for the application in Northeast China.

583 **Data availability.** Data are available from the corresponding author upon request  
584 (jiuengliu@hit.edu.cn).

585 **Author contributions.** YC and JL designed the study and prepared the paper, with inputs from all  
586 the co-authors. XC and ZZ carried out the experiments. SZ and HZ performed the simulations. QZ  
587 and KH validated the results and supervised the study.

588 **Competing interests.** At least one of the (co-)authors is a member of the editorial board of  
589 Atmospheric Chemistry and Physics. The peer-review process was guided by an independent editor,  
590 and the authors have also no other competing interests to declare.

591 **Disclaimer.** Publisher's note: Copernicus Publications remains neutral with regard to jurisdictional  
592 claims in published maps and institutional affiliations.

593 **Acknowledgements.** The authors thank Zhen-yu Du at the National Research Center for  
594 Environmental Analysis and Measurement and Lin-lin Liang at the Chinese Academy of  
595 Meteorological Sciences for their help in sample analysis.

596 **Financial support.** This research has been supported by the National Natural Science Foundation  
597 of China (grant no. 42222706), and the Fundamental Research Funds for the Central Universities.

## 598 **References**

599 Akagi, S. K., Craven, J. S., Taylor, J. W., McMeeking, G. R., Yokelson, R. J., Burling, I. R., Urbanski,  
600 S. P., Wold, C. E., Seinfeld, J. H., Coe, H., Alvarado, M. J., and Weise, D. R.: Evolution of  
601 trace gases and particles emitted by a chaparral fire in California, *Atmos. Chem. Phys.*, 12,  
602 1397–1421, <https://doi.org/10.5194/acp-12-1397-2012>, 2012.

603 Alexander, D. T. L., Crozier, P. A., and Anderson, J. R.: Brown carbon spheres in East Asian outflow  
604 and their optical properties, *Science*, 321, 833–836, <https://doi.org/10.1126/science.1155296>,  
605 2008.

606 Baumgardner, D., Popovicheva, O., Allan, J., Bernardoni, V., Cao, J., Cavalli, F., Cozic, J., Diapouli,  
607 E., Eleftheriadis, K., Genberg, P. J., Gonzalez, C., Gysel, M., John, A., Kirchstetter, T. W.,  
608 Kuhlbusch, T. A. J., Laborde, M., Lack, D., Müller, T., Niessner, R., Petzold, A., Piazzalunga,  
609 A., Putaud, J. P., Schwarz, J., Sheridan, P., Subramanian, R., Swietlicki, E., Valli, G., Vecchi,  
610 R., and Viana, M.: Soot reference materials for instrument calibration and intercomparisons: a  
611 workshop summary with recommendations, *Atmos. Meas. Tech.*, 5, 1869–1887,  
612 <https://doi.org/10.5194/amt-5-1869-2012>, 2012.

613 Bond, T. C., Doherty, S. J., Fahey, D. W., Forster, P. M., Berntsen, T., DeAngelo, B. J., Flanner, M.

614 G., Ghan, S., Krämer, B., Koch, D., Kinne, S., Kondo, Y., Quinn, P. K., Sarofim, M. C., Schultz,  
615 M. G., Schulz, M., Venkataraman, C., Zhang, H., Zhang, S., Bellouin, N., Guttikunda, S. K.,  
616 Hopke, P. K., Jacobson, M. Z., Kaiser, J. W., Klimont, Z., Lohmann, U., Schwarz, J. P., Shindell,  
617 D., Storelvmo, T., Warren, S. G., and Zender, C. S.: Bounding the role of black carbon in the  
618 climate system: a scientific assessment, *J. Geophys. Res.*, 118, 5380–5552,  
619 <https://doi.org/10.1002/jgrd.50171>, 2013.

620 Buffaloe, G. M., Lack, D. A., Williams, E. J., Coffman, D., Hayden, K. L., Lerner, B. M., Li, S. M.,  
621 Nuaaman, I., Massoli, P., Onasch, T. B., Quinn, P. K., and Cappa, C. D.: Black carbon  
622 emissions from in-use ships: a California regional assessment, *Atmos. Chem. Phys.*, 14, 1881–  
623 1896, <https://doi.org/10.5194/acp-14-1881-2014>, 2014.

624 Cappa, C. D., Lim, C. Y., Hagan, D. H., Coggon, M., Koss, A., Sekimoto, K., de Gouw, J., Onasch,  
625 T. B., Warneke, C., and Kroll, J. H.: Biomass-burning-derived particles from a wide variety of  
626 fuels – Part 2: effects of photochemical aging on particle optical and chemical properties,  
627 *Atmos. Chem. Phys.*, 20, 8511–8532, <https://doi.org/10.5194/acp-20-8511-2020>, 2020.

628 Cavalli, F., Viana, M., Yttri, K. E., Genberg, J., and Putaud, J. P.: Toward a standardized thermal-  
629 optical protocol for measuring atmospheric organic and elemental carbon: the EUSAAR  
630 protocol, *Atmos. Meas. Tech.*, 3, 79–89, <https://doi.org/10.5194/amt-3-79-2010>, 2010.

631 Chen, K. P., Raeofy, N., Lum, M., Mayorga, R., Woods, M., Bahreini, R., Zhang, H. F., and Lin, Y.  
632 H.: Solvent effects on chemical composition and optical properties of extracted secondary  
633 brown carbon constituents, *Aerosol Sci. Technol.*, 56, 917–930,  
634 <https://doi.org/10.1080/02786826.2022.2100734>, 2022.

635 Chen, L. J., Gao, Y., Ma, M. C., Wang, L. L., Wang, Q. L., Guan, S. H., Yao, X. H., and Gao, H. W.:  
636 Striking impacts of biomass burning on PM<sub>2.5</sub> concentrations in Northeast China through the  
637 emission inventory improvement, *Environ. Pollut.*, 318, 120835,  
638 <https://doi.org/10.1016/j.envpol.2022.120835>, 2023.

639 Chen, Q., Ikemori, F., Nakamura, Y., Vodicka, P., Kawamura, K., and Mochida, M.: Structural and  
640 light-absorption characteristics of complex water-insoluble organic mixtures in urban  
641 submicrometer aerosols, *Environ. Sci. Technol.*, 51, 8293–8303,  
642 <https://doi.org/10.1021/acs.est.7b01630>, 2017.

643 Chen, Y., and Bond, T. C.: Light absorption by organic carbon from wood combustion, *Atmos.*  
644 *Chem. Phys.*, 10, 1773–1787, <https://doi.org/10.5194/acp-10-1773-2010>, 2010.

645 Cheng, Y., Cao, X. B., Liu, J. M., Yu, Q. Q., Zhong, Y. J., Geng, G. N., Zhang, Q., and He, K. B.:  
646 New open burning policy reshaped the aerosol characteristics of agricultural fire episodes in  
647 Northeast China, *Sci. Total. Environ.*, 810, 52272,  
648 <https://doi.org/10.1016/j.scitotenv.2021.152272>, 2022.

649 Cheng, Y., Yu, Q., Liu, J., Cao, X., Zhong, Y., Du, Z., Liang, L., Geng, G., Ma, W., Qi, H., Zhang,  
650 Q., and He, K.: Dramatic changes in Harbin aerosol during 2018–2020: the roles of open  
651 burning policy and secondary aerosol formation, *Atmos. Chem. Phys.*, 21, 15199–15211,  
652 <https://doi.org/10.5194/acp-21-15199-2021>, 2021a.



- 653 Cheng, Z. Z., Atwi, K., El Hajj, O., Ijeli, I., Al Fischer, D., Smith, G., and Saleh, R.: Discrepancies  
654 between brown carbon light-absorption properties retrieved from online and offline  
655 measurements, *Aerosol Sci. Technol.*, 55, 92–103,  
656 <https://doi.org/10.1080/02786826.2020.1820940>, 2021b.
- 657 Chow, J. C., Watson, J. G., Chen, L. W. A., Arnott, W. P., and Moosmüller, H.: Equivalence of  
658 elemental carbon by thermal/optical reflectance and transmittance with different temperature  
659 protocols, *Environ. Sci. Technol.*, 38, 4414–4422, <https://doi.org/10.1021/es034936u>, 2004.
- 660 Chow, J. C., Watson, J. G., Chen, L. W. A., Chang, M. O., Robinson, N. F., Trimble, D., and Kohl,  
661 S.: The IMPROVE-A temperature protocol for thermal/optical carbon analysis: maintaining  
662 consistency with a long-term database, *J. Air Waste Manage. Assoc.*, 57, 1014–1023,  
663 <https://doi.org/10.3155/1047-3289.57.9.1014>, 2007.
- 664 Collier, S., Zhou, S., Onasch, T. B., Jaffe, D. A., Kleinman, L., Sedlacek, A. J., Briggs, N. L., Hee,  
665 J., Fortner, E., Shilling, J. E., Worsnop, D., Yokelson, R. J., Parworth, C., Ge, X. L., Xu, J. Z.,  
666 Butterfield, Z., Chand, D., Dubey, M. K., Pekour, M. S., Springston, S., and Zhang, Q.:  
667 Regional influence of aerosol emissions from wildfires driven by combustion efficiency:  
668 insights from the BBOP campaign, *Environ. Sci. Technol.*, 50, 8613–8622,  
669 <https://doi.org/10.1021/acs.est.6b01617>, 2016.
- 670 Corbin, J. C., Czech, H., Massabò, D., de Mongeot, F. B., Jakobi, G., Liu, F., Lobo, P., Mennucci,  
671 C., Mensah, A. A., Orasche, J., Pieber, S. M., Prévôt, A. S. H., Stengel, B., Tay, L. L., Zanatta,  
672 M., Zimmermann, R., El Haddad, I., and Gysel, M.: Infrared-absorbing carbonaceous tar can  
673 dominate light absorption by marine-engine exhaust, *npj Clim. Atmos. Sci.*, 2, 12,  
674 <https://doi.org/10.1038/s41612-019-0069-5>, 2019.
- 675 Gao, C. Y., Heald, C. L., Katich, J. M., Luo, G., and Yu, F. Q.: Remote aerosol simulated during the  
676 Atmospheric Tomography (ATom) campaign and implications for aerosol lifetime, *J. Geophys.*  
677 *Res. Atmos.*, 127, e2022JD036524, <https://doi.org/10.1029/2022JD036524>, 2022.
- 678 Garofalo, L. A., Pothier, M. A., Levin, E. J. T., Campos, T., Kreidenweis, S. M., and Farmer, D. K.:  
679 Emission and evolution of submicron organic aerosol in smoke from wildfires in the Western  
680 United States, *ACS Earth Space Chem.*, 3, 1237–1247,  
681 <https://doi.org/10.1021/acsearthspacechem.9b00125>, 2019.
- 682 Giannoni, M., Calzolari, G., Chiari, M., Cincinelli, A., Lucarelli, F., Martellini, T., and Nava, S.: A  
683 comparison between thermal-optical transmittance elemental carbon measured by different  
684 protocols in PM<sub>2.5</sub> samples, *Sci. Total Environ.*, 571, 195–205,  
685 <https://doi.org/10.1016/j.scitotenv.2016.07.128>, 2016.
- 686 Hecobian, A., Zhang, X., Zheng, M., Frank, N., Edgerton, E. S., and Weber, R. J.: Water-soluble  
687 organic aerosol material and the light-absorption characteristics of aqueous extracts measured  
688 over the Southeastern United States, *Atmos. Chem. Phys.*, 10, 5965–5977,  
689 <https://doi.org/10.5194/acp-10-5965-2010>, 2010.
- 690 Hodgson, A. K., Morgan, W. T., O'Shea, S., Bauguitte, S., Allan, J. D., Darbyshire, E., Flynn, M. J.,  
691 Liu, D., Lee, J., Johnson, B., Haywood, J. M., Longo, K. M., Artaxo, P. E., and Coe, H.: Near-  
692 field emission profiling of tropical forest and Cerrado fires in Brazil during SAMBBA 2012,

- 693 *Atmos. Chem. Phys.*, 18, 5619–5638, <https://doi.org/10.5194/acp-18-5619-2018>, 2018.
- 694 Hoffer, A., Tóth, A., Nyirő-Kósa, I., Pósfai, M., and Gelencsér, A.: Light absorption properties of  
695 laboratory-generated tar ball particles, *Atmos. Chem. Phys.*, 16, 239–246,  
696 <https://doi.org/10.5194/acp-16-239-2016>, 2016.
- 697 Hu, J. L., Chen, J. J., Ying, Q., and Zhang, H. L.: One-year simulation of ozone and particulate  
698 matter in China using WRF/CMAQ modeling system, *Atmos. Chem. Phys.*, 16, 10333–10350,  
699 <https://doi.org/10.5194/acp-16-10333-2016>, 2016a.
- 700 Hu, W. W., Hu, M., Hu, W., Jimenez, J. L., Yuan, B., Chen, W. T., Wang, M., Wu, Y. S., Chen, C.,  
701 Wang, Z. B., Peng, J. F., Zeng, L. M., and Shao, M.: Chemical composition, sources, and aging  
702 process of submicron aerosols in Beijing: contrast between summer and winter, *J. Geophys.*  
703 *Res. Atmos.*, 121, 1955–1977, <https://doi.org/10.1002/2015JD024020>, 2016b.
- 704 Koch, D., Schulz, M., Kinne, S., McNaughton, C., Spackman, J. R., Balkanski, Y., Bauer, S.,  
705 Berntsen, T., Bond, T. C., Boucher, O., Chin, M., Clarke, A., De Luca, N., Dentener, F., Diehl,  
706 T., Dubovik, O., Easter, R., Fahey, D. W., Feichter, J., Fillmore, D., Freitag, S., Ghan, S.,  
707 Ginoux, P., Gong, S., Horowitz, L., Iversen, T., Kirkevåg, A., Klimont, Z., Kondo, Y., Krol,  
708 M., Liu, X., Miller, R., Montanaro, V., Moteki, N., Myhre, G., Penner, J. E., Perlwitz, J., Pitari,  
709 G., Reddy, S., Sahu, L., Sakamoto, H., Schuster, G., Schwarz, J. P., Seland, Ø., Stier, P.,  
710 Takegawa, N., Takemura, T., Textor, C., van Aardenne, J. A., and Zhao, Y.: Evaluation of black  
711 carbon estimations in global aerosol models, *Atmos. Chem. Phys.*, 9, 9001–9026,  
712 <https://doi.org/10.5194/acp-9-9001-2009>, 2009.
- 713 Konovalov, I. B., Lvova, D. A., Beekmann, M., Jethva, H., Mikhailov, E. F., Paris, J.-D., Belan, B.  
714 D., Kozlov, V. S., Ciaïș, P., and Andreae, M. O.: Estimation of black carbon emissions from  
715 Siberian fires using satellite observations of absorption and extinction optical depths, *Atmos.*  
716 *Chem. Phys.*, 18, 14889–14924, <https://doi.org/10.5194/acp-18-14889-2018>, 2018.
- 717 Kumar, N. K., Corbin, J. C., Bruns, E. A., Massabó D., Slowik, J. G., Drinovec, L., Močnik, G.,  
718 Prati, P., Vlachou, A., Baltensperger, U., Gysel, M., El-Haddad, I., and Prévôt, A. S. H.:  
719 Production of particulate brown carbon during atmospheric aging of residential wood-burning  
720 emissions, *Atmos. Chem. Phys.*, 18, 17843–17861, [https://doi.org/10.5194/acp-18-17843-](https://doi.org/10.5194/acp-18-17843-2018)  
721 2018, 2018.
- 722 Lack, D. A., Moosmüller, H., McMeeking, G. R., Chakrabarty, R. K., and Baumgardner, D.:  
723 Characterizing elemental, equivalent black, and refractory black carbon aerosol particles: a  
724 review of techniques, their limitations and uncertainties, *Anal. Bioanal. Chem.*, 406, 99–122,  
725 <https://doi.org/10.1007/s00216-013-7402-3>, 2014.
- 726 Lambe, A. T., Cappa, C. D., Massoli, P., Onasch, T. B., Forestieri, S. D., Martin, A. T., Cummings,  
727 M. J., Croasdale, D. R., Brune, W. H., Worsnop, D. R., and Davidovits, P.: Relationship  
728 between oxidation level and optical properties of secondary organic aerosol, *Environ. Sci.*  
729 *Technol.*, 47, 6349–6357, <https://doi.org/10.1021/es401043j>, 2013.
- 730 Laskin, A., Laskin, J., and Nizkorodov, S. A.: Chemistry of atmospheric brown carbon, *Chem. Rev.*,  
731 115, 4335–4382, <https://doi.org/10.1021/cr5006167>, 2015.

- 732 Li, H. Y., Lamb, K. D., Schwarz, J. P., Selimovic, V., Yokelson, R. J., McMeeking, G. R., and May,  
733 A. A.: Inter-comparison of black carbon measurement methods for simulated open biomass  
734 burning emissions, *Atmos. Environ.*, 206, 156–169,  
735 <https://doi.org/10.1016/j.atmosenv.2019.03.010>, 2019.
- 736 Liu, P. F., Abdelmalki, N., Hung, H.-M., Wang, Y., Brune, W. H., and Martin, S. T.: Ultraviolet and  
737 visible complex refractive indices of secondary organic material produced by photooxidation  
738 of the aromatic compounds toluene and *m*-xylene, *Atmos. Chem. Phys.*, 15, 1435–1446,  
739 <https://doi.org/10.5194/acp-15-1435-2015>, 2015.
- 740 Liu, J., Lin, P., Laskin, A., Laskin, J., Kathmann, S. M., Wise, M., Caylor, R., Imholt, F., Selimovic,  
741 V., and Shilling, J. E.: Optical properties and aging of light-absorbing secondary organic  
742 aerosol, *Atmos. Chem. Phys.*, 16, 12815–12827, <https://doi.org/10.5194/acp-16-12815-2016>,  
743 2016a.
- 744 Liu, X. X., Zhang, Y., Huey, L. G., Yokelson, R. J., Wang, Y., Jimenez, J. L., Campuzano-Jost, P.,  
745 Beyersdorf, A. J., Blake, D. R., Choi, Y., St Clair, J. M., Crouse, J. D., Day, D. A., Diskin, G.  
746 S., Fried, A., Hall, S. R., Hanisco, T. F., King, L. E., Meinardi, S., Mikoviny, T., Palm, B. B.,  
747 Peischl, J., Perring, A. E., Pollack, I. B., Ryerson, T. B., Sachse, G., Schwarz, J. P., Simpson, I.  
748 J., Tanner, D. J., Thornhill, K. L., Ullmann, K., Weber, R. J., Wennberg, P. O., Wisthaler, A.,  
749 Wolfe, G. M., and Ziemba, L. D.: Agricultural fires in the southeastern U.S. during SEAC4RS:  
750 emissions of trace gases and particles and evolution of ozone, reactive nitrogen, and organic  
751 aerosol, *J. Geophys. Res. Atmos.*, 121, 7383–7414, <https://doi.org/10.1002/2016JD025040>,  
752 2016b.
- 753 Liu, J. M., Wang, P. F., Zhang, H. L., Du, Z. Y., Zheng, B., Yu, Q. Q., Zheng, G. J., Ma, Y. L., Zheng,  
754 M., Cheng, Y., Zhang, Q., and He, K. B.: Integration of field observation and air quality  
755 modeling to characterize Beijing aerosol in different seasons, *Chemosphere*, 242, 125195,  
756 <https://doi.org/10.1016/j.chemosphere.2019.125195>, 2020.
- 757 Liu, T. Y., Chan, A. W. H., and Abbatt, J. P. D.: Multiphase oxidation of sulfur dioxide in aerosol  
758 particles: implications for sulfate formation in polluted environments, *Environ. Sci. Technol.*,  
759 8, 4227–4242, <https://doi.org/10.1021/acs.est.0c06496>, 2021.
- 760 McClure, C. D., Lim, C. Y., Hagan, D. H., Kroll, J. H., and Cappa, C. D.: Biomass-burning-derived  
761 particles from a wide variety of fuels – Part 1: properties of primary particles, *Atmos. Chem.*  
762 *Phys.*, 20, 1531–1547, <https://doi.org/10.5194/acp-20-1531-2020>, 2020.
- 763 Moosmüller, H., Chakrabarty, R. K., and Arnott, W. P.: Aerosol light absorption and its measurement:  
764 a review, *J. Quant. Spectrosc. Radiat. Transf.*, 110, 844–878,  
765 <https://doi.org/10.1016/j.jqsrt.2009.02.035>, 2009.
- 766 Moteki, N., and Kondo, Y.: Dependence of laser-induced incandescence on physical properties of  
767 black carbon aerosols: measurements and theoretical interpretation, *Aerosol Sci. Technol.*, 44,  
768 663–675, <https://doi.org/10.1080/02786826.2010.484450>, 2010.
- 769 Ning, C. P., Gao, Y., Yu, H. R., Zhang, H. J., Geng, N. B., Cao, R., and Chen, J. P.: FT-ICR mass  
770 spectrometry for molecular characterization of water-insoluble organic compounds in winter  
771 atmospheric fine particulate matters, *J. Environ. Sci.*, 111, 51–60,

- 772 <https://doi.org/10.1016/j.jes.2020.12.017>, 2022.
- 773 Onasch, T. B., Trimborn, A., Fortner, E. C., Jayne, J. T., Kok, G. L., Williams, L. R., Davidovits, P.,  
774 and Worsnop, D. R.: Soot particle aerosol mass spectrometer: development, validation, and  
775 initial application, *Aerosol Sci. Technol.*, 46, 804–817,  
776 <https://doi.org/10.1080/02786826.2012.663948>, 2012.
- 777 Petzold, A., Ogren, J. A., Fiebig, M., Laj, P., Li, S. M., Baltensperger, U., Holzer-Popp, T., Kinne,  
778 S., Pappalardo, G., Sugimoto, N., Wehrli, C., Wiedensohler, A., and Zhang, X. Y.:  
779 Recommendations for reporting “black carbon” measurements, *Atmos. Chem. Phys.*, 13,  
780 8365–8379, <https://doi.org/10.5194/acp-13-8365-2013>, 2013.
- 781 Petzold, A., Schloesser, H., Sheridan, P. J., Arnott, W. P., Ogren, J. A., and Virkkula, A.: Evaluation  
782 of multiangle absorption photometry for measuring aerosol light absorption, *Aerosol Sci.*  
783 *Technol.*, 39, 40–51, <https://doi.org/10.1080/027868290901945>, 2005.
- 784 Piazzalunga, A., Bernardoni, V., Fermo, P., Valli, G., and Vecchi, R.: Technical note: On the effect  
785 of water-soluble compounds removal on EC quantification by TOT analysis in urban aerosol  
786 samples, *Atmos. Chem. Phys.*, 11, 10193–10203, <https://doi.org/10.5194/acp-11-10193-2011>,  
787 2011.
- 788 Pileci, R. E., Modini, R. L., Bertò M., Yuan, J., Corbin, J. C., Marinoni, A., Henzing, B., Moerman,  
789 M. M., Putaud, J. P., Spindler, G., Wehner, B., Müller, T., Tuch, T., Trentini, A., Zanatta, M.,  
790 Baltensperger, U., and Gysel-Beer, M.: Comparison of co-located refractory black carbon (rBC)  
791 and elemental carbon (EC) mass concentration measurements during field campaigns at several  
792 European sites, *Atmos. Meas. Tech.*, 14, 1379–1403, [https://doi.org/10.5194/amt-14-1379-](https://doi.org/10.5194/amt-14-1379-2021)  
793 2021, 2021.
- 794 Rosenfeld, D., and Woodley, W. L.: Deep convective clouds with sustained supercooled liquid water  
795 down to -37.5 °C. *Nature*, 405, 440–442, <https://doi.org/10.1038/35013030>, 2000.
- 796 Samset, B. H., Myhre, G., Herber, A., Kondo, Y., Li, S. M., Moteki, N., Koike, M., Oshima, N.,  
797 Schwarz, J. P., Balkanski, Y., Bauer, S. E., Bellouin, N., Berntsen, T. K., Bian, H., Chin, M.,  
798 Diehl, T., Easter, R. C., Ghan, S. J., Iversen, T., Kirkevåg, A., Lamarque, J. F., Lin, G., Liu, X.,  
799 Penner, J. E., Schulz, M., Seland, Ø., Skeie, R. B., Stier, P., Takemura, T., Tsigaridis, K., and  
800 Zhang, K.: Modelled black carbon radiative forcing and atmospheric lifetime in AeroCom  
801 Phase II constrained by aircraft observations, *Atmos. Chem. Phys.*, 14, 12465–12477,  
802 <https://doi.org/10.5194/acp-14-12465-2014>, 2014.
- 803 Schwarz, J. P., Gao, R. S., Fahey, D. W., Thomson, D. S., Watts, L. A., Wilson, J. C., Reeves, J. M.,  
804 Darbeheshti, M., Baumgardner, D. G., Kok, G. L., Chung, S. H., Schulz, M., Hendricks, J.,  
805 Lauer, A., Karcher, B., Slowik, J. G., Rosenlof, K. H., Thompson, T. L., Langford, A. O.,  
806 Loewenstein, M., and Aikin, K. C.: Single-particle measurements of midlatitude black carbon  
807 and light-scattering aerosols from the boundary layer to the lower stratosphere, *J. Geophys.*  
808 *Res.*, 111, D16207, <https://doi.org/10.1029/2006JD007076>, 2006.
- 809 Sharma, S., Leaitch, W. R., Huang, L., Veber, D., Kolonjari, F., Zhang, W., Hanna, S. J., Bertram,  
810 A. K., and Ogren, J. A.: An evaluation of three methods for measuring black carbon in Alert,  
811 Canada, *Atmos. Chem. Phys.*, 17, 15225–15243, <https://doi.org/10.5194/acp-17-15225-2017>,

812 2017.

813 State Council: Circular on Further Promoting the Pollution Prevention and Control Battle,  
814 [https://www.gov.cn/zhengce/2021-11/07/content\\_5649656.htm](https://www.gov.cn/zhengce/2021-11/07/content_5649656.htm), 2021.

815 Stohl, A., Aamaas, B., Amann, M., Baker, L. H., Bellouin, N., Berntsen, T. K., Boucher, O., Cherian,  
816 R., Collins, W., Daskalakis, N., Dusinska, M., Eckhardt, S., Fuglestvedt, J. S., Harju, M., Heyes,  
817 C., Hodnebrog, Ø., Hao, J., Im, U., Kanakidou, M., Klimont, Z., Kupiainen, K., Law, K. S.,  
818 Lund, M. T., Maas, R., MacIntosh, C. R., Myhre, G., Myriokefalitakis, S., Olivi é D., Quaas,  
819 J., Quennehen, B., Raut, J. C., Rumbold, S. T., Samset, B. H., Schulz, M., Seland, O., Shine,  
820 K. P., Skeie, R. B., Wang, S., Yttri, K. E., and Zhu, T.: Evaluating the climate and air quality  
821 impacts of short-lived pollutants, *Atmos. Chem. Phys.*, 15, 10529–10566,  
822 <https://doi.org/10.5194/acp-15-10529-2015>, 2015.

823 Sun, Y. L., He, Y., Kuang, Y., Xu, W. Y., Song, S. J., Ma, N., Tao, J. C., Cheng, P., Wu, C., Su, H.,  
824 Cheng, Y. F., Xie, C. H., Chen, C., Lei, L., Qiu, Y. M., Fu, P. Q., Croteau, P., and Worsnop, D.  
825 R.: Chemical differences between PM<sub>1</sub> and PM<sub>2.5</sub> in highly polluted environment and  
826 implications in air pollution studies, *Geophys. Res. Lett.*, 47, e2019GL086288,  
827 <https://doi.org/10.1029/2019GL086288>, 2020.

828 Tinorua, S., Denjean, C., Nabat, P., Pont, V., Arnaud, M., Bourrienne, T., Dias Alves, M., and  
829 Gardrat, E.: Two-year intercomparison of three methods for measuring black carbon  
830 concentration at a high-altitude research station in Europe, *EGUsphere*,  
831 <https://doi.org/10.5194/egusphere-2024-47>, 2024.

832 Uranishi, K., Ikemori, F., Shimadera, H., Kondo, A., and Sugata, S.: Impact of field biomass burning  
833 on local pollution and long-range transport of PM<sub>2.5</sub> in Northeast Asia, *Environ. Pollut.*, 244,  
834 414–422, <https://doi.org/10.1016/j.envpol.2018.09.061>, 2019.

835 Wang, H. C., Lu, K. D., Tan, Z. F., Chen, X. R., Liu, Y. H., and Zhang, Y. H.: Formation mechanism  
836 and control strategy for particulate nitrate in China, *J. Environ. Sci.*, 123, 476–486,  
837 <https://doi.org/10.1016/j.jes.2022.09.019>, 2023a.

838 Wang, P. F., Chen, K. Y., Zhu, S. Q., Wang, P., and Zhang, H. L.: Severe air pollution events not  
839 avoided by reduced anthropogenic activities during COVID-19 outbreak, *Resour. Conserv.*  
840 *Recycl.*, 158, 104814, <https://doi.org/10.1016/j.resconrec.2020.104814>, 2020.

841 Wang, X., Heald, C. L., Liu, J. M., Weber, R. J., Campuzano-Jost, P., Jimenez, J. L., Schwarz, J. P.,  
842 and Perring, A. E.: Exploring the observational constraints on the simulation of brown carbon,  
843 *Atmos. Chem. Phys.*, 18, 635–653, <https://doi.org/10.5194/acp-18-635-2018>, 2018.

844 Wang, Y. T., Zhao, Y., Liu, Y. M., Jiang, Y. Q., Zheng, B., Xing, J., Liu, Y., Wang, S., and Nielsen,  
845 C. P.: Sustained emission reductions have restrained the ozone pollution over China, *Nat.*  
846 *Geosci.*, 16, 967–974, <https://doi.org/10.1038/s41561-023-01284-2>, 2023b.

847 Wiedinmyer, C., Akagi, S. K., Yokelson, R. J., Emmons, L. K., Al-Saadi, J. A., Orlando, J. J., and  
848 Soja, A. J.: The Fire INventory from NCAR (FINN): a high resolution global model to estimate  
849 the emissions from open burning, *Geosci. Model Dev.*, 4, 625–641,  
850 <https://doi.org/10.5194/gmd-4-625-2011>, 2011.

851 Wu, X., Cao, F., Haque, M., Fan, M. Y., Zhang, S. C., and Zhang, Y. L.: Molecular composition and  
852 source apportionment of fine organic aerosols in Northeast China, *Atmos. Environ.*, 239,  
853 117722, <https://doi.org/10.1016/j.atmosenv.2020.117722>, 2020.

854 Xiao, Q., Zheng, Y., Geng, G., Chen, C., Huang, X., Che, H., Zhang, X., He, K., and Zhang, Q.:  
855 Separating emission and meteorological contributions to long-term PM<sub>2.5</sub> trends over eastern  
856 China during 2000–2018, *Atmos. Chem. Phys.*, 21, 9475–9496, [https://doi.org/10.5194/acp-](https://doi.org/10.5194/acp-21-9475-2021)  
857 21-9475-2021, 2021.

858 Xie, X. C., Zhang, Y. Z., Liang, R. S., Chen, W., Zhang, P. X., Wang, X., Zhou, Y., Cheng, Y., and  
859 Liu, J.M.: Wintertime heavy haze episodes in Northeast China driven by agricultural fire  
860 emissions, *Environ. Sci. Technol. Lett.*, 11, 150–157,  
861 <https://doi.org/10.1021/acs.estlett.3c00940>, 2024.

862 Yan, F. P., Kang, S. C., Sillanpää M., Hu, Z. F., Gao, S. P., Chen, P. F., Gautam, S., Reinikainen, S.  
863 P., and Li, C. L.: A new method for extraction of methanol-soluble brown carbon: implications  
864 for investigation of its light absorption ability, *Environ. Pollut.*, 262, 114300,  
865 <https://doi.org/10.1016/j.envpol.2020.114300>, 2020.

866 Yang, M., Howell, S. G., Zhuang, J., and Huebert, B. J.: Attribution of aerosol light absorption to  
867 black carbon, brown carbon, and dust in China - Interpretations of atmospheric measurements  
868 during EAST-AIRE, *Atmos. Chem. Phys.*, 9, 2035–2050, [https://doi.org/10.5194/acp-9-2035-](https://doi.org/10.5194/acp-9-2035-2009)  
869 2009, 2009.

870 Ying, Q, Li, J. Y, and Kota, S. H.: Significant contributions of isoprene to summertime secondary  
871 organic aerosol in eastern United States, *Environ. Sci. Technol.*, 49, 7834–7842,  
872 <https://doi.org/10.1021/acs.est.5b02514>, 2019.

873 Zeng, L. H., Dibb, J., Scheuer, E., Katich, J. M., Schwarz, J. P., Bourgeois, I., Peischl, J., Ryerson,  
874 T., Warneke, C., Perring, A. E., Diskin, G. S., DiGangi, J. P., Nowak, J. B., Moore, R. H.,  
875 Wiggins, E. B., Pagonis, D., Guo, H. Y., Campuzano-Jost, P., Jimenez, J. L., Xu, L., and Weber,  
876 R. J.: Characteristics and evolution of brown carbon in western United States wildfires, *Atmos.*  
877 *Chem. Phys.*, 22, 8009–8036, <https://doi.org/10.5194/acp-22-8009-2022>, 2022.

878 Zhang, J., Liu, L., Xu, L., Lin, Q., Zhao, H., Wang, Z., Guo, S., Hu, M., Liu, D., Shi, Z., Huang, D.,  
879 and Li, W.: Exploring wintertime regional haze in northeast China: role of coal and biomass  
880 burning, *Atmos. Chem. Phys.*, 20, 5355–5372, <https://doi.org/10.5194/acp-20-5355-2020>,  
881 2020.